2006-07-08

DNA-Templated Surface Alignment and Characterization of Carbon Nanotubes.

Huijun Xin
Brigham Young University - Provo

DNA-TEMPLATED SURFACE ALIGNMENT AND CHARACTERIZATION OF CARBON NANOTUBES

by

Huijun Xin

A dissertation submitted to the faculty of

Brigham Young University

in partial fulfillment of the requirements for the degree of

Doctor of Philosophy

Department of Chemistry and Biochemistry

Brigham Young University

December 2006

BRIGHAM YOUNG UNIVERSITY

GRADUATE COMMITTEE APPROVAL

of a dissertation submitted by

Huijun Xin

This dissertation has been read by each member of the following graduate committee and by majority vote has been found to be satisfactory.

Date	Adam T. Woolley, Chair
Date	Matthew R. Linford
Date	David V. Dearden
Date	Steven R. Goates
Date	Steven W. Graves

BRIGHAM YOUNG UNIVERSITY

As chair of the candidate's graduate committee, I have read the dissertation of Huijun Xin in its final form and have found that (1) its format, citations, and bibliographical style are consistent and acceptable and fulfill university and department style requirements; (2) its illustrative materials including figures, and charts are in place; and (3) the final manuscript is satisfactory to the graduate committee and is ready for submission to the university library.

_____ _____

Date

Adam T. Woolley
Chair, Graduate Committee

Accepted for the Department

_____

David V. Dearden
Graduate Coordinator

Accepted for the College

_____

Tom Sederberg
Associate Dean, College of Physical and Mathematical Science

ABSTRACT

DNA-TEMPLATED SURFACE ALIGNMENT

AND CHARACTERIZATION OF

CARBON NANOTUBES

Huijun Xin

Department of Chemistry and Biochemistry

Doctor of Philosophy

Carbon nanotubes are appealing materials for nanofabrication due to their unique properties and structures. However, for carbon nanotubes to be used in mass-fabricated devices, precise control of nanotube orientation and location on surfaces is critical.

I have developed a technique to align single-walled carbon nanotubes (SWNTs) on surfaces from a droplet of nanotube suspension under gas flow. Fluid motion studies indicate that alignment is likely due to circulation of SWNTs in the droplet. My work provides a facile method for generating oriented nanotubes for nanodevice applications.

I have also devised an approach for localizing SWNTs onto 1-pyrenemethylamine-decorated DNA on surfaces. I found that 63% of SWNTs on surfaces were anchored along DNA, and these nanotubes covered ~5% of the total DNA length. This technique was an initial demonstration of DNA-templated SWNT localization.

In an improved method to localize SWNTs on DNA templates, dodecyltrimethylammonium bromide was utilized to suspend SWNTs in aqueous media and localize them on DNA electrostatically. SWNT positioning was controlled by the surface DNA arrangement, and the extent of deposition was influenced by the SWNT concentration and number of treatments. Under optimized conditions, 83% of the length of surface DNAs was covered with SWNTs, and 76% of the deposited SWNTs were on DNA. In some regions, nearly continuous SWNT assemblies were formed. This approach should be useful for the fabrication of nanotube nanowires in nanoelectronic circuits.

Using my improved procedures, I have localized SWNTs on DNA templates across electrodes and measured the electrical properties of DNA-templated SWNT assemblies. When a DNA-templated SWNT was deposited on top of and bridging electrodes, the measured conductance was comparable to literature values. In contrast, SWNTs with end-on contacts to the sides of electrodes had conductances hundreds of times lower than literature values, probably due to gaps between the SWNT ends and the electrodes.

This work provides a novel approach for localizing SWNTs across contacts in a controlled manner. These results may be useful in the fabrication of nanoelectronic devices such as transistors with SWNTs as active components. Moreover, this approach could be valuable in arranging SWNTs as electrical interconnects for nanoelectronics applications.

ACKNOWLEDGEMENTS

First of all, I thank my advisor Dr. Adam T. Woolley for his patience and effective mentoring. I also thank my graduate committee members, Dr. Matthew R. Linford, Dr. David V. Dearden, Dr. Steven R. Goates, and Dr. Steven W. Graves for their valuable suggestions. Second, I specially thank Hector A. Becerril. He designed and fabricated the microelectrodes used in nanotube conductance studies, and gave me many helpful suggestions for my experiments. I thank Dr. Ryan T. Kelly and Tao Pan for their experimental assistance. I also thank Dr. Woolley's group members for their useful discussions and friendship. Moreover, I thank the Army Research Laboratory and the U.S. Army Research Office for funding this work. I thank the Brigham Young University Chemistry and Biochemistry Department for giving me the chance to study here. Finally, I thank my parents, my husband, Jianguo, and my daughters, Emily and Olivia, for their support.

TABLE OF CONTENTS

LIST OF FIGURES

LIST OF TABLES

CHAPTER 1: INTRODUCTION

1.1 Nanofabrication and Nanoelectronics

Nanofabrication is the controlled design and manufacture of features with dimensions at the nanometer scale. Nanofabrication has attracted attention in a variety of fields, including medicine, the military, the aerospace industry, computing, etc. In this section, I will focus on bottom-up nanofabrication methods for electronic applications.

Progress in the fabrication of integrated circuits (ICs) has resulted in an increase in performance and decrease in costs in the electronics industry. The enhancement of the speed and performance of ICs is in part related to a reduction in their critical dimensions. Moore's first law states that the number of transistors per square centimeter on an IC doubles every two years without an increase in the cost [1]. This law has largely held true in the fabrication of ICs for several decades, and at the present time, top-down micromachining techniques are widely applied. These top-down methods are a set of tools, by which smaller devices are constructed from bigger building blocks. Examples of top-down fabrication tools include photolithography, thin-film deposition, electrochemical machining, wet or dry etching, and electrothermal or mechanical processes.

However, conventional top-down approaches are encountering an increasing

number of challenges and limitations that may hinder adherence to Moore's law. Thus, researchers have begun to explore bottom-up methodologies as alternative approaches to nanofabrication. In bottom-up techniques, bigger structures are built up using smaller building blocks, such as atoms or molecules. Indeed, the self-assembly of biological molecules is an important manufacturing method in bottom-up nanotechnology, enabling building blocks to assemble into desired structures. Some advantages of bottom-up methods include potential low cost, ability to use a variety of materials, and the possibility of building sophisticated devices.

Molecular electronics, where molecular-scale objects serve as key elements in electronic devices, is an active area of research. A conducting molecular wire was reported by Weiss and coworkers [2] in 1996. In their fabrication, a conjugated molecule, a 4,4'-di(phenylene-ethynylene)-benzenethiolate derivative, was inserted into an insulating *n*-dodecanethiol monolayer on gold to form a single molecule wire. Subsequently, Weiss's group [3] used scanning tunneling microscopy (STM) to study conductance switching in phenylene ethynylene oligomers. They found that a conformational change of single or bundled molecules resulted in conductance switching. Metzger's group [4] found that a zwitterionic monolayer of hexadecylquinolinium tricyanoquinodimethanide acted as a rectifier of electrical current between oxide-free Au electrodes. They measured a maximum rectification ratio of 27.5 and a maximum current of 9.04×10^4 electrons molecule^{-1} s^{-1}. Hsu et al. [5] inserted an alkanedithiol molecular layer between Au and GaAs electrodes to form a diode. Their studies of this molecular diode showed that internal photoemission electrons resulted from the occupied levels of the GaAs-molecular interfacial states. A lot of promising work has been done in

molecular electronics, but big challenges still exist. For example, only simple device geometries are understood theoretically; devices with more complex structures still need to be studied. In addition, chemical reactions may occur during electrical transport through molecules.

Carbon nanotubes (CNTs), because of their unique electronic properties and dimensions, have received increased attention for the fabrication of nanoelectronics. Dai's group made individual single-walled carbon nanotube (SWNT) field-effect transistors (FETs) by growing SWNTs on patterned substrates, and then functionalizing the SWNT sidewalls with polyethylene imines [6]. This amine-rich polymer resulted in n-type FETs. Manohara et al. used angled evaporation to deposit titanium (Schottky contact) and platinum (Ohmic contact) at the ends of a semiconducting SWNT to fabricate Schottky diodes [7]. These SWNT diodes exhibited ideality factors (the slopes of their current-voltage plots, as measured on a semi-logarithmic scale) ranging from 1.5 to 1.9, indicating reasonable electronic properties. Rogers' group presented the construction of SWNT thin-film transistors that exhibited high device mobility of 3-40 cm^2/Vs and on/off ratios of 100-1000 [8]. If one half of a device is coated with poly(methyl methacrylate) and the other half with polyethylenimine, the device can function as a p-n diode. Avouris et al. developed techniques to obtain n-type CNT-FETs by annealing p-type CNT-FETs, which allowed them to fabricate SWNT inter- and intramolecular logic gates having both n-type and p-type CNT-FETs [9]. These logic gates could change an input of 1 to an output 0, or vice versa. Keren et al. used a bottom-up approach to localize a CNT at a specific position within a DNA molecule and then

metallized the DNA on both sides of the CNT to form a CNT-FET [10]. This work utilized DNA as a template, and took advantage of self-assembly nature of biomolecules.

1.2 Carbon Nanotubes

1.2.1 Introduction

In 1991, Sujio Iijima discovered a novel carbon material [11], which is now called the multi-walled carbon nanotube (MWNT). Two years later, Iijima and Ichihasshi reported the discovery of SWNTs [12]. Since then, the study of CNTs has been pursued heavily.

CNTs have tubular structures. A SWNT is a sheet of graphene that is rolled into a cylinder and has half fullerenes capping the ends. The diameter of a SWNT is typically on the order of 1-5 nm. MWNTs are composed of several concentric graphene cylinders with typical diameters of 10-50 nm. Both types of CNTs can have lengths from <100 nm to the centimeter range [13].

The structure of a SWNT can be characterized by a roll-up vector $\mathbf{c_h}$ and a chiral angle θ, as shown in Figure 1.1 [14]. The roll-up vector $\mathbf{c_h}$ is:

$$\mathbf{c_h} = n\mathbf{a_1} + m\mathbf{a_2} \equiv (n, m) \tag{1.1}$$

where $\mathbf{a_1}$ and $\mathbf{a_2}$ are the graphene lattice vectors, and n and m are integers. The values of n and m classify nanotubes into three categories.

$$n = m \qquad \text{Armchair} \tag{1.2}$$

$$n = 0 \text{ or } m = 0 \qquad \text{Zigzag} \tag{1.3}$$

$$n \neq m, \text{ for } n \text{ or } m \neq 0 \qquad \text{Chiral} \tag{1.4}$$

The chiral angle θ indicates the direction of the roll-up vector, and is defined as the angle

between $\mathbf{a_1}$ and $\mathbf{c_h}$ [15]. The chiral angle can be calculated from the following formula:

$$\cos\theta = \frac{a_1 \cdot c_h}{|a_1| \cdot |c_h|} = \frac{n + m/2}{\sqrt{n^2 + nm + m^2}} \tag{1.5}$$

Zigzag nanotubes (n, 0) have a chiral angle $\theta = 0°$, while armchair nanotubes (n, n) have a chiral angle $\theta = 30°$. Both zigzag and armchair nanotubes are achiral.

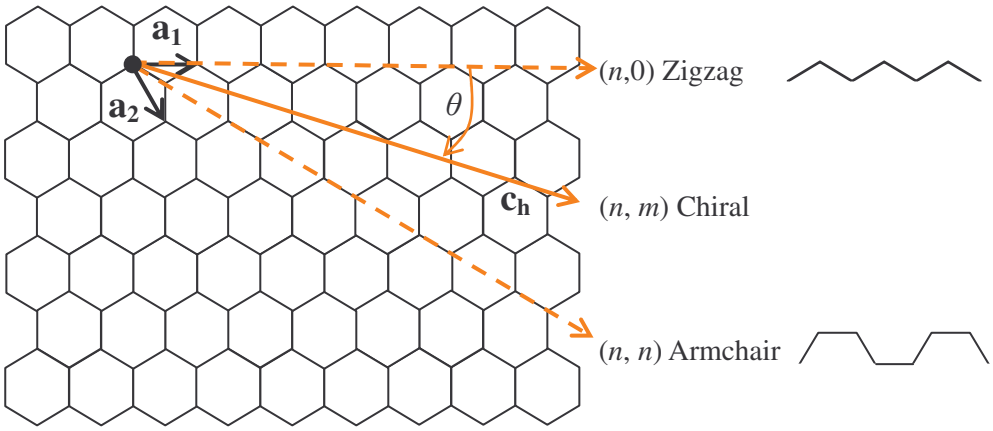

Figure 1.1 Schematic diagram of a two-dimensional graphene sheet, indicating vectors $\mathbf{a_1}$, $\mathbf{a_2}$, $\mathbf{c_h}$, and θ, and vectors showing zigzag, armchair, and chiral tubes. Adapted with permission from [14]; copyright 1998 Nature Publishing Group.

1.2.2 Electronic Properties

In 1992, based on theoretical calculations, several groups predicted that SWNTs could be metallic or semiconducting depending on helicity and diameter [16-20]. These papers suggested that: (1) for zigzag SWNTs, when $n/3$ is an integer, the tubes should behave as a metal; otherwise, they should be semiconductors; (2) armchair SWNTs should be metallic; and (3) chiral SWNTs can be metallic or semiconducting depending on the values of n and m. Chiral SWNTs are metallic when $(2n+m)/3$ is an integer; otherwise, they are semiconducting.

In 1998, Lieber's group and Dekker's group explored both the atomic structure and electronic properties of individual SWNTs using STM and scanning tunneling spectroscopy [14, 21, 22]. These experiments confirmed the existence of metallic and semiconducting SWNTs and further demonstrated that the electronic properties of SWNTs indeed depended on diameter and helicity as predicted by theory. Both groups also observed 1D van Hove singularities [21, 22] in the normalized conductance, which confirmed the one-dimensional nature of conduction within SWNTs. Lieber's group also determined that the band gap of semiconducting SWNTs depended inversely on nanotube diameter [21].

Dekker's group pioneered the study of electrical transport in individual SWNTs, with potential nanodevice applications. For individual metallic SWNTs, electrical conduction occurred through discrete electronic states at low temperature, indicating that these SWNTs behaved as quantum wires [23]. The fabrication of a FET using a single semiconducting SWNT connected to two Pt electrodes was also reported by Dekker's group [24]. The SWNT was modulated from conducting to insulating when a voltage was applied to the gate electrode. The device, a room-temperature transistor, was compared to models for traditional semiconductor devices. These transport studies revealed potential applications of semiconducting SWNTs in molecular electronics.

For a metallic SWNT with perfect electrical contacts, two units of quantum conductance are expected as:

$$G = 2G_0 = 4e^2/h = 150\ \mu S \tag{1.6}$$

where e is the electron charge and h is Planck's constant; this conductance corresponds a resistance of 6.5 kΩ [25, 26]. Resistances of individual metallic SWNTs as high as 1 MΩ

[23] to 2.9 MΩ [27] have been reported. The high resistances were likely due to imperfect contacts of the SWNTs with the electrodes. By matching the metal contact work function to the SWNTs, Dai and coworkers observed conductances of metallic SWNTs with lengths <1 μm approaching $2G_0$ [28], confirming the ballistic transport nature in metallic SWNTs.

Heer's group described the quantum behavior of MWNTs [29]. They found that MWNTs conduct current ballistically, and they measured the conductance of MWNTs to be ~1 G_0 (75 μS). McEuen's group determined a resistance of 42 kΩ for a MWNT with a diameter of 9 nm [30]. Avouris et al. demonstrated that MWNTs did not show gating effects in a FET design, but deformed MWNTs could operate as FETs [25].

1.2.3 Physical Properties

Carbon nanotubes have high stiffness and axial strength due to their seamless cylindrical graphitic structures. Young's modulus values for MWNTs of ~1.8 TPa [31] and ~1.3 TPa [32] have been measured with different instruments. The Young's modulus of SWNTs was determined to be ~1.25 TPa [33]. The high Young's modulus of CNTs indicates that they are considerably stiffer than hardened steel (210 GPa).

The tensile strength of CNTs (how much force they can carry before breaking) was evaluated by Rouff's group. MWNTs exhibited tensile strengths in the range of 11-63 GPa [34], and the average tensile strength for an individual SWNT was 30 GPa [35]. These measurements indicate that CNTs can withstand much greater tension than high-grade steel, which has a 1.6 GPa tensile strength [36].

The thermal conductivity of CNTs has been studied with equilibrium and nonequilibrium molecular dynamics simulations. Goddard's group used equilibrium

molecular dynamics to calculate the thermal conductivity of CNTs [37], while Tománek's group combined equilibrium and nonequilibrium molecular dynamics simulations [38]. Both groups found that the thermal conductivity of CNTs was very high (>3000 W/m K) and comparable to that of diamond. Tománek's group also determined that the thermal conductivity of CNTs was dependent on temperature, and they attributed the high CNT thermal conductivity to large phonon mean free paths.

1.2.4 Chemical Properties

1.2.4.1 Noncovalent Functionalization

Noncovalent functionalization can readily be done on the sidewalls of CNTs. Dai and coworkers noncovalently deposited a bifunctional molecule, 1-pyrenebutanoic acid, on the sidewalls of SWNTs [39]. They suggested that the interaction was due to π-stacking between the SWNT surface and the pyrenyl groups. After the SWNTs were functionalized with 1-pyrenebutanoic acid, the proteins streptavidin and ferritin were localized on the SWNTs. I have used a similar technique to place SWNTs on DNA [40]. A bifunctional compound, 1-pyrenemethylamine (PMA), was anchored on DNA first through electrostatic interactions. Then, due to π-stacking effects between the SWNT sidewalls and the pyrenyl groups of PMA, SWNTs were localized on surface DNA.

Another type of noncovalent functionalization of CNTs utilizes the hydrophobic nature of the CNT surface. Mioskowski and colleagues studied the hydrophobic interactions between MWNTs and streptavidin [41], and found that MWNTs could be almost completely coated with this protein. Ajayan's group coated CNT surfaces with multiple polymer layers [42]. A first layer of poly(amphiphiles) was coated on CNTs through hydrophobic interactions, and then a second polymer layer was cross-linked onto

the first layer. Through covalent or electrostatic interactions, more polymer layers were attached on CNTs, which allowed the localization of gold nanoparticles on CNTs.

1.2.4.2 Covalent Functionalization

Many covalent functionalizations of CNTs start with a nitric acid oxidation to produce carboxylic acid groups either at the ends or in defects on the sidewalls of nanotubes. Oxidized CNTs can then be functionalized at their carboxylic acid groups by esterification and amidation reactions to attach alkyl chains [43], polymers [44, 45], etc.

Different functional groups have been attached to CNTs. Mickelson et al. developed a chemical method to fluorinate and defluorinate SWNT sidewalls at different temperatures [46]. Tour's group reported a solvent-free technique to functionalize SWNTs and MWNTs with aryl chloride, bromide, ester, nitro, and tert-butyl moieties [47]. This technique allowed large-scale derivatization of CNTs. Hirsch's group functionalized SWNT sidewalls with (R-)oxycarbonyl nitrene [48], which allowed subsequent covalent attachment of many groups, including alkyl chains, aromatics, dendrimers, crown ethers, and oligoethylene glycols. Haddon's group modified SWNT sidewalls with dichlorocarbene, creating attached -CCl_2 groups [49]. Tour et al. derivatized small-diameter (0.7 nm) SWNTs with aryl diazonium salts, based on an electrochemical reduction reaction, which led to aryl radicals attached on SWNT surfaces [50].

A main purpose of functionalization of CNTs is to enhance their solubility in aqueous or organic solvents. When SWNTs were derivatized with glucosamine through amide bond formation, the resultant products could be dispersed in water [51]. Alkylation of SWNT sidewalls using lithium and alkyl halides made the nanotubes more soluble in chloroform, tetrahydrofuran, and *N,N*-dimethylformamide [52].

Functionalization of CNTs with biomolecules, such as nucleic acids, peptides, and proteins, can enable further applications. Nguyen and coworkers derivatized the open ends of vertical MWNT arrays with nucleic acids, making a nanoelectrode biosensor platform to detect complementary DNA molecules [53]. Sun et al. attached bovine serum albumin (BSA) to SWNTs and MWNTs [54]. CNTs were oxidized to produce carboxylic acids, and BSA proteins were bound to CNTs through diimide-activated amidation; importantly, the CNT-attached BSA displayed bioactivity in total protein micro-determination assays. This technique might increase the biocompatibility of CNTs and enable their use in vivo. In a potential vaccine delivery application, Bianco and coworkers attached peptides to CNTs using two strategies: fragment condensation of fully protected peptides and selective chemical ligation [55]. The peptide-CNT conjugates were demonstrated to elicit an immune response.

1.2.5 Summary of Why Carbon Nanotubes Are Well Suited for Nanoelectronics

Carbon nanotubes, depending on helicity and diameter, can behave as metals or semiconductors. Metallic nanotubes can act as nanowires, and semiconducting nanotubes can serve as transistors in nanoelectronic devices. CNTs are also extremely strong and stiff materials with good thermal conductivity. Chemical functionalization methods allow CNTs to become soluble in aqueous solution or interact selectively with target compounds. These electrical, physical, and chemical characteristics make CNTs appealing candidates for use in nanoelectronics.

1.3 DNA as a Nanofabrication Template

1.3.1 DNA Structure

Deoxyribonucleic acid (DNA) is a double-helical polymer, composed of two intertwined strands. The monomer units of each DNA strand are called nucleotides. A nucleotide consists of a 5-carbon sugar (deoxyribose), a nitrogenous base, and a phosphate group. There are four different types of bases in DNA: adenine (A), guanine (G), cytosine (C), and thymine (T). To form the double-helix structure of DNA, two polynucleotide strands bind together through hydrogen bonds formed between specific pairs of bases on different strands: A pairs with T, and G pairs with C. Thus, the base sequence in one strand determines the bases in the strand that will be complementary. The diameter of double-stranded (ds) DNA is ~2.0-2.4 nm [56], and its length ranges from a few nanometers to hundreds of micrometers.

λ DNA is a linear, double-stranded molecule, 48,502 base pairs in size with an extended length of ~16 μm [57]. There is a 12-base single-stranded (ss) DNA segment at each end of the strands. These ssDNA ends are complementary in sequence, and when hybridized they convert λ DNA into a circular molecule. The length of λ DNA makes it well-suited to be a scaffold in connecting micrometer-scale features, and the "sticky ends" allow it to hybridize with complementary sequences to construct complex structures. Thus, λ DNA is employed extensively as a template in bottom-up nanofabrication, as described in Sections 1.3.3 and 1.3.4 in this chapter.

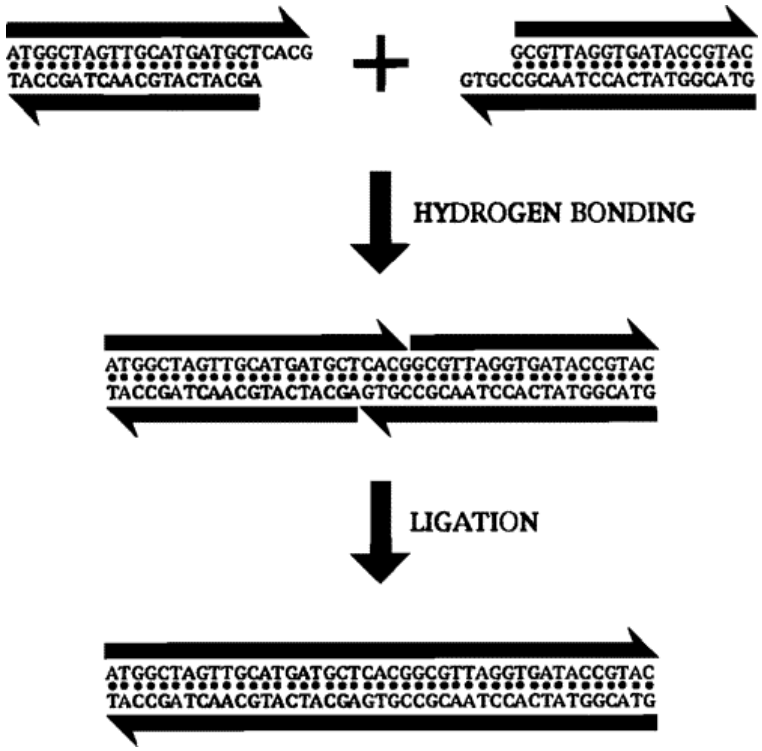

Figure 1.2 Diagram of sticky-ended cohesion and ligation. Reprinted with permission from [58]; copyright 1997 American Chemical Society.

The specific molecular recognition properties of nucleic acids make the self-assembly of DNA nanostructures possible. Seeman and coworkers were the first to design complex structures with DNA molecules using sticky-ended association [58]; Figure 1.2 shows an example of this approach, where two dsDNA molecules are designed with complementary ends. Under appropriate conditions, the sticky ends bind to each other to form a longer DNA molecule. If ligase enzymes and cofactors are added, the new DNA molecule is joined covalently. By taking advantage of this sticky-ended association, Seeman et al. designed a series of sophisticated structures based on DNA molecules [59, 60], involving three-, four-, five- and six-arm branched DNA junctions, as well as molecular architectures [58], such as DNA cubes, knots, pentagonal dodecahedra, and

borromean rings. These reports demonstrate the possibility of using DNA components to construct complex nanoscale structures.

1.3.2 DNA Alignment

One potential nanotechnology application of DNA is in serving as a nanowire template; often, DNA needs to be aligned on a surface first. A variety of approaches have been investigated to elongate DNA on different substrates. In the spin-stretching method, a $MgCl_2$-soaked mica substrate was spin coated with a DNA solution [61], and the DNA was aligned on the surface by centrifugal forces. Li et al. developed a convenient method to elongate DNAs on mica surfaces [62]. They used a gas flow stream to drive a droplet of DNA on an unmodified mica substrate, leaving the DNA molecules aligned on the surface. The flow direction and the speed of the moving droplet affected the DNA alignment. In another simple method, a drop of DNA solution was aspirated from a polymer-coated glass substrate using a micropipette [63]. Air-water interface motion induced by aspiration made DNA molecules align radially on the surface. An approach developed in Woolley's group is as follows [64]. A three-axis micromanipulator was used to hold a glass coverslip, which was brought into gentle contact with a droplet of DNA solution resting on a Si substrate. Motion of the coverslip caused the droplet to move on the surface, aligning the DNA on the surface in any desired direction. Other methods involving either magnetic [65], laser-optical [56], or dielectric forces [66] have also been used to align DNA molecules on surfaces.

1.3.3 DNA-Templated Metallization

Metallization of aligned surface DNA is one bottom-up approach to form nanowires. In this method, DNA molecules are first elongated on a surface, and then a

solution containing metal ions is allowed to interact with the DNA for several minutes. Finally, the associated metal ions are chemically transformed to neutral atoms with a reducing reagent.

The first DNA-templated metal nanowires were made by Braun and coworkers [67]. They affixed two different sequences (complimentary to the two 12-base sticky ends of λ DNA) to two microfabricated gold electrodes. λ DNA was aligned across the electrodes, and the sticky ends base paired with the surface-attached oligonucleotides. Silver ions were exchanged with other cations associated with the λ DNA and then were reduced to silver atoms using hydroquinone. The resulting Ag nanowires had diameters of ~100 nm. Current vs. voltage (I-V) measurements showed that there were zero-current plateaus at low voltage, but with increasing voltage, the wires became conductive. Resistances of 30 MΩ and 7 MΩ were measured for two nanowires. Braun et al.'s work established the feasibility of constructing nanowires using DNA as a template.

Since this initial demonstration, researchers have placed efforts on coating DNA templates with various metals. Palladium metallization of DNA was first shown by Richter and coworkers [68]. They observed quasi-continuous Pd coating on DNA, with metallic features having a diameter of 20-40 nm. Mao et al. reported the construction of parallel and crossed palladium nanowire arrays on DNA templates, with average nanowire diameters of 30 nm [69]. In one approach for Au metallization of DNA, gold nanoparticles were coated with positively charged groups first, which made them interact electrostatically with DNA. Nakao et al. reported continuous deposition of aniline-capped Au nanoparticles on DNA [70]. Woolley's group investigated the fabrication of DNA-templated Ag and Cu nanowires [71, 72]. By employing a background reduction

technique, they were the first to make linear metal nanostructures on single-stranded DNA templates. Electroless plating is another method for placing metals on DNA, and Ford et al. used this technique to deposit Pt on DNA [73]. Although they observed gaps between Pt nanoparticles, they expected that the Pt-coated DNA could act as a seed layer for subsequent deposition of other metals.

1.3.4 DNA-Templated SWNT Localization

CNTs have unique structural, chemical and electronic properties, which make them appealing materials for nanotechnology applications. However, localizing CNTs on surfaces in a controlled manner remains a challenge. One bottom-up approach is to use surface-aligned DNA as a template to place CNTs in well-arranged surface arrays.

Braun et al. localized a semiconducting SWNT at a desired position on a DNA molecule [10]. In this method, RecA protein was first attached on ssDNA to form a nucleoprotein filament, which was then bound to the complementary section within dsDNA. This assembly was treated with biotinylated anti-RecA antibodies. SWNTs were dispersed in aqueous sodium dodecyl sulfate (SDS) solution and were functionalized with streptavidin. A streptavidin-coated SWNT was bound to the desired section of the dsDNA through biotin-streptavidin interaction. Once the unmodified sections of DNA had been metallized with silver, a DNA-templated SWNT FET was fabricated.

I developed two methods to localize SWNTs on DNA [40, 74], which will be described in greater detail in Chapters 3 and 4. In the first approach, PMA was positioned on surface-aligned DNA due to the electrostatic interaction between the PMA amine group and the DNA phosphate backbone. Then, SWNTs were localized on the PMA/DNA assembly due to hydrophobic interactions between the PMA pyrene groups

and SWNT surfaces. In the second method, a cationic surfactant, dodecyltrimethylammonium bromide (DTAB), was utilized. When SWNTs were suspended in a DTAB solution, they were encased inside micelle-like DTAB structures. The DTAB-wrapped SWNTs were then positioned on surface DNA molecules through electrostatic interactions between the positively charged DTAB head groups and the negatively charged DNA backbone.

In Braun et al.'s approach, SWNTs were localized on a specific dsDNA segment, while in my method, SWNTs were placed nonspecifically on the DNA. Importantly, my approach is simpler and has potential for continuous coating of DNA with SWNTs.

1.4 Atomic Force Microscopy

1.4.1 Introduction

In 1986, Binnig, Quate, and Gerber first demonstrated atomic force microscopy (AFM) [75], which combined the principles of operation of STM and the stylus profilometer. AFM measures the force between a sharp tip and a sample substrate to obtain an image of the surface topography. These forces are very small, typically from 10^{-11} to 10^{-6} N. AFM employs an optical technique to detect these small forces (Figure 1.3). The AFM tip is located on the end of a cantilever, and when the tip scans a substrate,

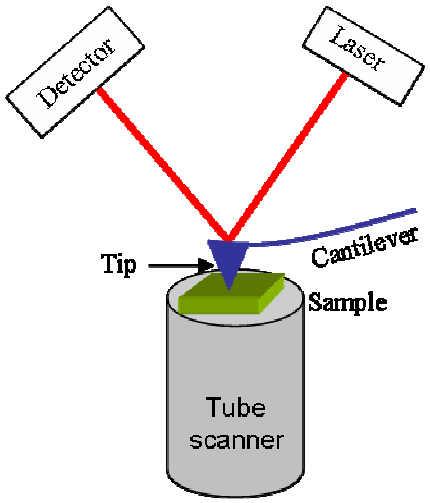

Figure 1.3 A diagram showing the principle of deflection detection.

the force between the tip and the surface causes the cantilever to bend. The bending of the cantilever is monitored by detecting the deflection of the laser beam at a quadrant photodiode. Typical cantilever spring constants are in the range of 0.001-100 N/m. The optimal deflection method can measure motions from micrometers to 0.1 Å, corresponding to forces as little as 0.01 pN.

1.4.2 Operation Modes of AFM

Three main operation modes for AFM are contact, tapping, or non-contact mode. In contact mode, as the tip scans the sample, the interatomic force between the tip and surface is repulsive. Contact mode offers higher lateral resolution and scan speeds than the other two AFM modes. One drawback of this mode is that large lateral forces can be applied on the sample during imaging, which may damage the surface or alter the topography of sensitive specimens. Contact mode is best suited for samples with relatively hard features.

In tapping mode (also called intermittent contact mode), the tip makes periodic contact with the surface as the cantilever is oscillated at or near the resonance frequency. An important advantage of tapping mode is that lateral forces are reduced, so the sample is less likely to be damaged by the tip. Tapping mode is used widely in the analysis of biological and soft samples.

In non-contact mode, the tip operates at a distance of tens to hundreds of angstroms above a sample, where the tip-surface force is attractive. Because there is no contact between the tip and the sample, there is no the lateral force on the sample. This mode has relatively slow imaging speed and is usually used for probing hydrophobic samples.

1.4.3 Resolution and Tip

The two different spatial resolution considerations in an AFM image are lateral (X, Y) and vertical (Z) resolution. The lateral resolution is primarily determined by the radius of curvature of the end of the tip, while the vertical resolution is dictated by the resolution of the vertical scanner movement, which is typically very precise (<1 Å). Given specific AFM instrumentation, the vertical resolution cannot be changed, but the lateral resolution can be improved by using a sharper tip. Considerable effort has focused on the development of sharper tips [76-79]. At present, typical AFM tips are made of silicon nitride (Si_3N_4) or silicon and have an end radius in the range of 10-30 nm. The sharpest available tips have an end radius around 5 nm.

One way to make a sharper AFM tip is to attach a SWNT to the tip end, such that the protruding SWNT acts as the tip [77]. Since SWNTs can have an end radius <1 nm, SWNT tips can greatly improve the lateral resolution in AFM imaging. Lieber's group has developed two approaches to fabricate SWNT tips for AFM imaging. In the first method, CNTs were grown directly on the ends of commercial AFM tips [78]. The grown CNTs were shortened to minimize vibration, and a CNT protruding from the end of the cantilever acted as the tip. In an alternative SWNT tip fabrication approach, SWNTs were grown vertically from planar substrate surfaces; then, individual SWNTs were picked up from the substrate when the tip imaged the surface [79]. With the second technique, SWNTs could be attached to new AFM tips or to worn-out AFM tips, such that older tips could be reused by picking up a new SWNT for imaging.

1.4.4 Advantages and Disadvantages of AFM

Compared to transmission electron microscopy (TEM), AFM has three advantages. First, AFM generates a three-dimensional surface profile, while TEM only provides a two-dimensional image. Second, AFM does not require any special treatment (e.g., to enhance conductivity) that may alter the samples. Finally, AFM works in an air or liquid environment, while a TEM operates in ultrahigh vacuum. However, there are still advantages of TEM over AFM. For instance, TEM can probe the interior of structures, unlike AFM. In addition, AFM image resolution strongly depends on the shape of the AFM tip, while TEM has no tip effects.

Compared to STM, AFM can be used for conducting and insulating surfaces, while STM can only image conducting surfaces. However, STM resolution is usually higher than in AFM, because the tunneling current strongly depends on distance.

AFM has some advantages compared to scanning electron microscopy (SEM), in addition to those already detailed above in comparison to TEM. First, AFM can obtain atomic-resolution images, while SEM has a resolution on the order of a few nanometers. Second, AFM can perform in-situ imaging on samples that closely approximate in vivo conditions. One main disadvantage of AFM compared to SEM is the image size. SEM can probe an area and a depth of field on the order of millimeters, while ~150 × 150 μm is the largest area imaged with AFM, and the maximum height is ~15 μm. In addition, the scanning speed of AFM is much slower than SEM, although new advances have increased the AFM image acquisition rate [80].

1.4.5 Applications of AFM

AFM has been used in investigating a broad range of samples. He et al. used AFM

to observe transferrin-mediated cellular uptake of gold nanoparticles by nasopharyngeal carcinoma cells [81]. Braun et al. studied DNA-templated Ag nanowires with AFM [67]. Liu and coworkers explored the *Escherichia coli* outer membrane with AFM [82]. The AFM images showed vertical resolution of 5 Å and lateral resolution of 50 Å, which enabled them to observe detailed features of *E. coli* cells. Okumura et al. studied the growth of bimetallic Pt-Rh crystallites on single-crystal α-Al_2O_3 substrates with AFM [83]. Norrman et al. investigated the thickness and surface coverage of poly(methyl methacrylate) and poly(vinyl chloride) thin films on silicon wafers with AFM [84]. Jensen and coworkers deposited SWNTs on As surfaces and then grew (Ga, Mn)As, which acted as leads [85]. AFM images indicated that the SWNTs were incorporated in single crystal semiconductors, forming SWNT-semiconductor electronic devices. Using in-situ AFM imaging, Hansma and colleagues observed dynamic movement of extracellular matrix glycoproteins [86].

Research has also been done based on force measurements with AFM. For example, Hoh et al. investigated the forms of neurofilament sidearms by analyzing AFM force-distance measurements [87]. They suggested that an entropic brush from neurofilament sidearms maintained the interfilament spacing. Georgiou et al. measured the force between *E. coli* bacteria and hydrophilic or hydrophobic glass substrates, which were coated with poly(ethylene glycol)-lysine dendron and Pluronic F127 [88]. They found that the polymers blocked the long-range attractive forces of interaction and produced short-range repulsive steric interactions between the bacteria and the surface. Sharma et al. studied the adhesion forces between *E. coli* bacteria and biomaterial surfaces [89]. They attached *E. coli* cells to AFM tip, and then measured the force

between the tip and various substrates: mica, hydrophilic or hydrophobic glass, polystyrene and Teflon. Their AFM results agreed with theoretical predictions that bacterial adhesion should depend on the surface hydrophobicity.

In addition, AFM can be used to manipulate nanostructures. Koel et al. fabricated three-dimensional structures by positioning individual nanoparticles using an AFM tip [90, 91]. Dekker's group used an AFM tip to drag individual metallic CNTs and fabricate a room-temperature single-electron transistor [92]. Avouris et al. demonstrated a more complex manipulation of CNTs with an AFM tip [93]; they straightened, translated, bent, and cut CNTs, demonstrating a range of tip-based operations on nanotubes.

Since it was invented in 1986, the AFM technique has been improved greatly. Its advantages of high resolution, providing three-dimensional information, in-situ performance in fluids, and imaging conducting or non-conducting surfaces enable it to be applied in many fields.

1.5 Dissertation Overview

I have focused on developing effective methods for arranging SWNTs on surfaces in a controlled manner. Chapter 2 describes my work on SWNT alignment on surfaces from a droplet of nanotube suspension under gas flow. Orthogonally aligned arrays of SWNTs were also fabricated in a two-step process. I developed two approaches to place SWNTs on DNA templates, which are presented in Chapters 3 and 4. In Chapter 3, I used PMA as a bridging compound between DNA and SWNTs. The amine group of PMA interacted attractively with the negatively charged phosphate backbone of DNA, while the pyrenyl group in PMA interacted with SWNT surfaces through π-stacking forces. In

Chapter 4, a cationic surfactant, DTAB, was utilized to suspend SWNTs in aqueous media and localize them on DNA through electrostatic interactions. SWNT positioning was controlled by the surface DNA arrangement, and the extent of deposition was influenced by the SWNT concentration. Using this method, DNA coverage with SWNTs was improved by an order of magnitude compared to the earlier approach, and nearly continuous SWNT assemblies were achieved. Chapter 5 presents results with electronic property characterization of DNA-templated SWNTs aligned across electrodes. I-V curves were obtained, and under appropriate conditions the measured conductances of SWNTs were close to literature values. Finally, I present conclusions and discuss potential future work in Chapter 6.

1.6 References

1. Madou, M. J. Fundamentals of Microfabrication: The Science of Miniaturization, 2nd edn, Boca Raton, FL: CRC Press, **2002**.
2. Bumm, L. A.; Arnold, J. J.; Cygan, M. T.; Dunbar, T. D.; Burgin, T. P.; Jones, L., II; Allara, D. L.; Tour, J. M.; Weiss, P. S. Are Single Molecular Wires Conducting? *Science* **1996**, *271*, 1705-1701.
3. Donhauser, Z. J.; Mantooth, B. A.; Kelly, K. F.; Bumm, L. A.; Monnell, J. D.; Stapleton, J. J.; Price, D. W., Jr.; Rawlett, A. M.; Allara, D. L.; Tour, J. M.; Weiss, P. S. Conductance Switching in Single Molecules through Conformational Changes, *Science* **2001**, *292*, 2303-2307.
4. Metzger, R. M.; Xu, T.; Peterson, I. R. Electrical Rectification by a Monolayer of Hexadecylquinolinium Tricyanoquinodimethanide Measured between Macroscopic Gold Electrodes, *J. Phys. Chem. B* **2001**, *105*, 7280-7290.
5. Hsu, J. W. P.; Lang, D. V.; West, K. W.; Loo, Y.-L.; Halls, M. D.; Raghavachari, K. Probing Occupied States of the Molecule Layer in Au-Alkanedithiol-GaAs Diodes, *J. Phys. Chem. B* **2005**, *109*, 5719-5723.
6. Shim, M.; Javey, A.; Kam, N. W. S.; Dai, H. J. Polymer Functionalization for Air-Stable n-Type Carbon Nanotube Field-Effect Transistors, *J. Am. Chem. Soc.* **2001**, *123*, 11512-11513.
7. Manohara, H. M.; Wong, E. W.; Schlecht, E.; Hunt, B. D.; Siegel, P. H. Carbon Nanotube Schottky Diodes Using Ti-Schottky and Pt-Ohmic Contacts for High Frequency Applications, *Nano Lett.* **2005**, *5*, 1469-1474.

8. Zhou, Y.; Gaur, A.; Hur, S.-H.; Kocabas, C.; Meitl, M. A.; Shim, M.; Rogers, J. A. p-Channel, n-Channel Thin Film Transistors and p-n Diodes Based on Single Wall Carbon Nanotube Networks, *Nano Lett.* **2004**, *4*, 2031-2035.
9. Derycke, V.; Martel, R.; Appenzeller, J.; Avouris, Ph. Carbon Nanotube Inter- and Intramolecular Logic Gates, *Nano Lett.* **2001**, *1*, 453-456.
10. Keren, K.; Berman, R. S.; Buchstab, E.; Sivan, U. Braun, E. DNA-Templated Carbon Nanotube Field-Effect Transistor, *Nature* **2003**, *302*, 1380-1382.
11. Iijima, S. Helical Microtubules of Graphitic Carbon. *Nature* **1991**, *354*, 56-58.
12. Iijima, S.; Ichihasshi, T. Single-Shell Carbon Nanotubes of 1-nm Diameter, *Nature* **1993**, *363*, 603-605.
13. Dai, H. Carbon Nanotubes: Opportunities and Challenges, *Surf. Sci.* **2002**, *500*, 218-241.
14. Odom, T. W.; Huang, J. L.; Kim, P.; Lieber, C. M. Atomic Structure and Electronic Properties of Single-Walled Carbon Nanotubes, *Nature* **1998**, *391*, 62-64.
15. Reich, S.; Thomsen, C.; Maultzsch, T. J. *Carbon Nanotubes: Basic Concepts and Physical Properties*, Wiley-VCH Verlag GmbH, Weinheim, Germany, **2004**.
16. Mintmire, J. W.; Dunlap, B. I.; White, C. T. Are Fullerene Tubules Metallic? *Phys. Rev. Lett.* **1992**, *68*, 631-634.
17. Hamada, N.; Sawada, S.; Oshiyama, A. N. New One-Dimensional Conductors: Graphitic Microtubules, *Phys. Rev. Lett.* **1992**, *68*, 1579-1581.
18. Saito, R.; Fujita, M.; Dresselhaus, G.; Dresselhaus, M. S. Electronic Structure of Chiral Graphene Tubules, *Appl. Phys. Lett.* **1992**, *60*, 2204-2206.
19. Saito, R.; Fujita, M.; Dresselhaus, G.; Dresselhaus, M. S. Electronic Structure of

Graphene Tubules Based on C_{60}, *Phys. Rev. B* **1992**, *46*, 1804-1811.

20. White, C. T.; Robertson, D. H.; Mintmire, J. W. Helical and Rotational Symmetries of Nanoscale Graphitic Tubules, *Phys. Rev. B* **1993**, *47*, 5485-5488.
21. Odom, T. W.; Huang, J.-L.; Kim, P.; Quyang, M.; Lieber, C. M. Scanning Tunneling Microscopy and Spectroscopy Studies of Single Wall Carbon Nanotubes, *J. Mater. Res.* **1998**, *13*, 2380-2398.
22. Wildoer, J. W. G.; Venema, L. C.; Rinzler, A. G.; Smalley, R. E.; Dekker, C. Electronic Structure of Atomically Resolved Carbon Nanotubes, *Nature* **1998**, *391*, 59-62.
23. Tans, S. J.; Devoret, M. H.; Dai, H. J.; Thess, A.; Smalley, R. E.; Geerligs, L. J.; Dekker, C. Individual Single-Wall Carbon Nanotubes as Quantum Wires, *Nature* **1997**, *386*, 474-477.
24. Tans, S. J.; Verschueren R. M.; Dekker, C. Room-Temperature Transistor Based on a Single Carbon Nanotube, *Nature* **1998**, *393*, 49-52.
25. Dekker, C. Carbon Nanotubes as Molecular Quantum Wires, *Phys. Today* **1999**, *52*, 22-28.
26. White, C. T.; Todorov, T. N. Carbon Nanotubes as Long Ballistic Conductors, *Nature* **1998**, *393*, 240-242.
27. Martel, R.; Schmidt, T.; Shea, H. R.; Hertel, T.; Avouris, Ph. Single- and Multi-Wall Carbon Nanotube Field-Effect Transistors, *Appl. Phys. Lett.* **1998**, *73*, 2447-2449.
28. Kong, J.; Yenilmez, E.; Tombler, T.; Kim, W.; Liu, L.; Wu, S. Y.; Laughlin, J. R.; Dai, H. Quantum Interference and Ballistic Transmission in Nanotube Electron Waveguides, *Phys. Rev. Lett.* **2001**, *87*, 106801-106804.

29. Frank, S.; Poncharal, P.; Wang, Z. L.; Heer, W. A. Carbon Nanotube Quantum Resistors, *Science* **1998**, *280*, 1744-1746.

30. Bachtold, A.; Fuhrer, M. S.; Plyasunov, S.; Forero, M.; Anderson, E. H.; Zettl, A.; McEuen, P. L. Scanned Probe Microscopy of Electronic Transport in Carbon Nanotubes, *Phys. Rev. Lett.* **2000**, *84*, 6082-6085.

31. Treacy, M. M. J.; Ebbesen, T. W.; Gibson, J. M. Exceptionally High Young's Modulus Observed for Individual Carbon Nanotubes, *Nature* **1996**, *381*, 678-680.

32. Wong, E. W.; Sheehan, P. E.; Lieber, C. M. Nanobeam Mechanics: Elasticity, Strength, and Toughness of Nanorods and Nanotubes, *Science* **1997**, *277*, 1971-1975.

33. Krishnan, A.; Dujardin, E.; Ebbesen, T. W.; Yianilos, P. N.; Treacy, M. M. J. Young's Modulus of Single-Walled Nanotubes, *Phys. Rev. B* **1998**, *58*, 14013-14019.

34. Yu, M.-F.; Oleg Lourie, O.; Dyer, M. J.; Moloni, K.; Kelly, T. F.; Ruoff, R. S. Strength and Breaking Mechanism of Multiwalled Carbon Nanotubes under Tensile Load, *Science* **2000**, *287*, 637-640.

35. Yu, M.-F.; Files, B. S.; Arepalli, S.; Ruoff, R. S. Tensile Loading of Ropes of Single Wall Carbon Nanotubes and their Mechanical Properties, *Phys. Rev. Lett.* **2000**, *84*, 5552-5555.

36. http://www.geocities.com/pganio/materials.html (accessed April 8, 2006).

37. Che, J.; Cagin, T.; Goddard, W. A., III. Thermal Conductivity of Carbon Nanotubes, *Nanotechnology* **2002**, *11*, 65-69.

38. Savas Berber, S.; Kwon, Y.-K.; Tománek, D. Unusually High Thermal Conductivity of Carbon Nanotubes, *Phys. Rev. Lett.* **2000**, *84*, 4613-4616.

39. Chen, R. J.; Zhang, Y.; Wang, D.; Dai, H. Noncovalent Sidewall Functionalization of

Single-Walled Carbon Nanotubes for Protein Immobilization, *J. Am. Chem. Soc.* **2001**, *123*, 3838-3839.

40. Xin, H.; Woolley, A. T. DNA-Templated Nanotube Localization, *J. Am. Chem. Soc.* **2003**, *125*, 8710-8711.
41. Balavoine, F.; Schultz, P.; Richard, C.; Mallouh, V.; Ebbesen, T. W.; Mioskowski, C. Helical Crystallization of Proteins on Carbon Nanotubes: A First Step Towards the Development of New Biosensors, *Angew. Chem., Int. Ed.* **1999**, *38*, 13-14.
42. Carrillo, A.; Swartz, J. A.; Gamba, J. M.; Kane, R. S.; Chakrapani, N.; Wei, B.; Ajayan, P. M. Noncovalent Functionalization of Graphite and Carbon Nanotubes with Polymer Multilayers and Gold Nanoparticles, *Nano Lett.* **2003**, *3*, 1437-1440.
43. Chen, J.; Hamon, M. A.; Hu, H.; Chen, Y. S.; Rao, A. M.; Eklund, P. C.; Haddon, R. C. Solution Properties of Single-Walled Carbon Nanotubes, *Science* **1998**, *282*, 95-98.
44. Qin, S.; Qin, D.; Ford, W. T.; Resasco, D. E.; Herrera, J. E. Polymer Brushes on Single-Walled Carbon Nanotubes by Atom Transfer Radical Polymerization of *n*-Butyl Methacrylate, *J. Am. Chem. Soc.* **2004**, *126*, 170-176.
45. Riggs, J. E.; Guo, Z.; Carroll, D. L.; Sun, Y. P. Strong Luminescence of Solubilized Carbon Nanotubes, *J. Am. Chem. Soc.* **2000**, *122*, 5879-5880.
46. Mickelson, E. T.; Huffman, C. B.; Rinzler, A. G.; Smalley, R. E.; Hauge, R. H.; Margrave, J. L. Fluorination of Single-Wall Carbon Nanotubes, *Chem. Phys. Lett.* **1998**, *296*, 188-194.
47. Dyke, C. A.; Tour, J. M. Solvent-Free Functionalization of Carbon Nanotubes, *J. Am. Chem. Soc.* **2003**, *125*, 1156-1157.
48. Holzinger, M.; Abraham, J.; Whelan, P.; Graupner, R.; Ley, L.; Hennrich, F.; Kappes,

M.; Hirsch, A. Functionalization of Single-Walled Carbon Nanotubes with (R-)Oxycarbonyl Nitrenes, *J. Am. Chem. Soc.* **2003**, *125*, 8566-8580.

49. Hu, H.; Zhao, B.; Hamon, M. A.; Kamaras, K.; Itkis, M. E.; Haddon, R. C. Sidewall Functionalization of Single-Walled Carbon Nanotubes by Addition of Dichlorocarbene, *J. Am. Chem. Soc.* **2003**, *125*, 14893-14900.
50. Bahr, J. L.; Yang, J. P.; Kosynkin, D. V.; Bronikowski, M. J.; Smalley, R. E.; Tour, J. M. Functionalization of Carbon Nanotubes by Electrochemical Reduction of Aryl Diazonium Salts: A Bucky Paper Electrode, *J. Am. Chem. Soc.* **2001**, *123*, 6536-6542.
51. Pompeo, F.; Resasco, D. E. Water Solubilization of Single-Walled Carbon Nanotubes by Functionalization with Glucosamine, *Nano Lett.* **2002**, *2*, 369-373.
52. Liang, F.; Sadana, A. K.; Peera, A.; Chattopadhyay, J.; Gu, Z.; Hauge, R. H.; Billups, W. E. A Convenient Route to Functionalized Carbon Nanotubes, *Nano Lett.* **2004**, *4*, 1257-1260.
53. Nguyen, C. V.; Delzeit, L.; Cassell, A. M.; Li, J.; Han, J.; Meyyappan, M. Preparation of Nucleic Acid Functionalized Carbon Nanotube Arrays, *Nano Lett.* **2002**, *2*, 1079-1081.
54. Huang, W.; Taylor, S.; Fu, K.; Lin, Y.; Zhang, D.; Hanks, T. W.; Rao, A. M.; Sun, Y.-P. Attaching Proteins to Carbon Nanotubes via Diimide-Activated Amidation, *Nano Lett.* **2002**, *2*, 311-314.
55. Pantarotto, D.; Partidos, C. D.; Graff, R.; Hoebeke, J.; Briand, J.-P.; Prato, M.; Bianco, A. Synthesis, Structural Characterization, and Immunological Properties of Carbon Nanotubes Functionalized with Peptides, *J. Am. Chem. Soc.* **2003**, 125, 6160-6164.

56. Delmonte, C. S.; Mann, L. R. B. Variety in DNA Secondary Structure, *Current Science* **2003**, *85*, 1564-1570.

57. Smith, S. B.; Cui, Y.; Bustamante, C. Overstretching B-DNA: The Elastic Response of Individual Double-Stranded and Single-Stranded DNA Molecules, *Science* **1996**, *271*, 795-799.

58. Seeman, N. C. DNA Components for Molecular Architecture, *Acc. Chem. Res.* **1997**, *30*, 357-363.

59. Ma, R.; Kallenbach, N. R.; Sheardy, R. D.; Petrillo, M. L.; Seeman, N. C. Three-Arm Nucleic Acid Junctions Are Flexible, *Nucleic Acids Res.* **1986**, *14*, 9745-9752.

60. Wang, Y.; Mueller, J. E.; Kemper, B.; Seeman, N. C. Nanoscale Palladium Metallization of DNA, *Biochemistry* **1991**, *30*, 5667-5674.

61. Yokota, H.; Sunwoo, J.; Sarikaya, M.; Engh G.; Aebersold, R. Spin-Stretching of DNA and Protein Molecules for Detection by Fluorescence and Atomic Force Microscopy, *Anal. Chem.* **1999**, *71*, 4418-4422.

62. Li, J.; Bai, C.; Wang, C.; Zhu, C.; Lin, Z.; Li, Q.; Cao, E. A Convenient Method of Aligning Large DNA Molecules on Bare Mica Surfaces for Atomic Force Microscopy, *Nucleic Acids Res.*, **1998**, *26*, 4785-4786.

63. Nakao, H.; Hayashi, H.; Yoshino, T.; Sugiyama, S.; Otobe, K.; Ohtani, T. Development of Novel Polymer-Coated Substrates for Straightening and Fixing DNA, *Nano Lett.* **2002**, *2*, 475-479.

64. Woolley, A. T.; Kelly, R. T. Deposition and Characterization of Extended Single-Stranded DNA Molecules on Surfaces, *Nano Lett.* **2001**, *1*, 345-348.

65. Smith, S. B.; Finzi, L; Bustamante, C. Direct Mechanical Measurements of the Elasticity of Single DNA Molecules by Using Magnetic Beads, *Science* **1992**, *258,* 1122-1126.

66. Smith, S. B.; Aldridge, P. D.; Callis, J. B. Observation of Individual DNA Molecules Undergoing Gel Electrophoresis, *Science* **1989**, *243*, 203-206.

67. Braun, E.; Eichen, Y.; Sivan, U.; Ben-Yoseph, G. DNA-Templated Assembly and Electrode Attachment of a Conducting Silver Wire, *Nature* **1998**, *391*, 775-778.

68. Richter, J.; Seidel, R.; Kirsch, R.; Mertig, M.; Pompe, W.; Plaschke, J.; Schackert, H. K. Nanoscale Palladium Metallization of DNA, *Adv. Mater.* **2000**, *12*, 507-510.

69. Deng, Z.; Mao, C. DNA-Templated Fabrication of 1D Parallel and 2D Crossed Metallic Nanowire Arrays, *Nano Lett.* **2003**, *3*, 1545-1548.

70. Nakao, H.; Shiigi, H.; Yamamoto, Y.; Tokonami, S.; Nagaoka, T.; Sugiyama, S.; Ohtani, T. Highly Ordered Assemblies of Au Nanoparticles Organized on DNA, *Nano lett.* **2003**, *3*, 1391-1394.

71. Monson, C. F.; Woolley, A. T. DNA-Templated Construction of Copper Nanowires, *Nano Lett.* **2003**, *3*, 359-363.

72. Becerril, H. A.; Stoltenberg, R. M.; Monson, C. F.; Woolley, A. T. Ionic Surface Masking for Low Background in Single- and Double-Stranded DNA-Templated Silver and Copper Nanorods, *J. Mater. Chem.* **2004**, *14***,** 611-616.

73. Ford, W. E.; Harnack, O.; Yasuda, A.; Wessels, J. M. Platinated DNA as Precursors to Templated Chains of Metal Nanoparticles, *Adv. Mater.* **2001**, *13*, 1793-1797.

74. Xin, H.; Woolley, A. T. High-Yield DNA-Templated Assembly of Surfactant-Wrapped Carbon Nanotubes, *Nanotechnology* **2005**, *16*, 2238-2241.

75. Binnig, G.; Quate, C. F. Atomic Force Microscope, *Phys. Rev. Lett.* **1986**, *56*, 930-933.

76. Martinez, J.; Yuzvinsky, T. D.; Fennimore, A. M.; Zettl, A.; Garcia, R.; Bustamante, C. Length Control and Sharpening of Atomic Force Microscope Carbon Nanotube Tips Assisted by an Electron Beam, *Nanotechnology* **2005**, *16*, 2493-2496.

77. Wong, S. S.; Woolley, A. T.; Joselevich, E.; Cheung, C. L.; Lieber, C. M. Covalently-Functionalized Single-Walled Carbon Nanotube Probe Tips for Chemical Force Microscopy, *J. Am. Chem. Soc.* **1998**, *120*, 8557-8558.

78. Hafner, J. H.; Cheung, C.-L.; Lieber, C. M. Direct Growth of Single-Walled Carbon Nanotube Scanning Probe Microscopy Tips, *J. Am. Chem. Soc.* **1999**, *121*, 9750-9751.

79. Hafner, J. H.; Cheung, C.-L.; Oosterkamp, T. H.; Lieber, C. M. High-Yield Assembly of Individual Single-Walled Carbon Nanotube Tips for Scanning Probe Microscopies, *J. Phys. Chem. B* **2001**, *105*, 743-746.

80. Park, H.-K.; Hong, Y. K.; Lee, S. Q.; Moon, K. S. Design of an Compact Atomic Force Microscope to Enhance Scanning Speed, Proceedings of the SPIE International Conference on Opto-mechatronic Actuators, Sensors and Control, SPIE, Philadelphia, Vol. 5602, pp. 196-202, **2004**.

81. Yang, P.-H.; Sun, X.; Chiu, J.-F.; Sun, H.; He, Q.-Y. Transferrin-Mediated Gold Nanoparticle Cellular Uptake, *Bioconjugate Chem.* **2005**, *16*, 494-496.

82. Amro, N. A.; Kotra, L. P.; Wadu-Mesthrige, K.; Bulychev, A.; Mobashery, S.; Liu,

G.-Y. High-Resolution Atomic Force Microscopy Studies of the *Escherichia coli* Outer Membrane: Structural Basis for Permeability, *Langmuir* **2000**, *16*, 2789-2796.

83. Okumura, K.; Hyodo, S.; Noda, S.; Maruyama, Y. Growth of Pt-Rh Alloy Crystallites on α-Al_2O_3 Studied by Atomic Force Microscopy and Rutherford Backscattering Spectroscopy, *J. Phys. Chem. B* **1998**, *102*, 2350-2355.
84. Norrman, K.; Haugshoj, K. B.; Larsen, N. B. Lateral and Vertical Quantification of Spin-Coated Polymer Films on Silicon by TOF-SIMS, XPS, and AFM, *J. Phys. Chem. B* **2002**, *106*, 13114-13121.
85. Jensen, A.; Hauptmann, J. R.; Nygard, J.; Sadowski, J.; Lindelof, P. E. Hybrid Devices from Single Wall Carbon Nanotubes Epitaxially Grown into a Semiconductor Heterostructure, *Nano Lett.* **2004**, *4*, 349-352.
86. Chen, H.; Clegg, D.; Hansma, H. Structures and Dynamic Motion of Laminin-1 as Observed by Atomic Force Microscopy, *Biochemistry* **1998**, *37*, 8262-8267.
87. Brown, H. G.; Hoh, J. H. Entropic Exclusion by Neurofilament Sidearms: A Mechanism for Maintaining Interfilament Spacing, *Biochemistry* **1997**, *36*, 15035-15040.
88. Razatos, A.; Ong, Y.-L.; Boulay, F.; Elbert, D. L.; Hubbell, J. A.; Sharma, M. M.; Georgiou, G. Force Measurements between Bacteria and Poly(ethylene glycol)-Coated Surfaces, *Langmuir* **2000**, *16*, 9155-9158.
89. Ong, Y.-L.; Razatos, A.; Georgiou, G.; Sharma, M. M. Adhesion Forces between *E. coli* Bacteria and Biomaterial Surfaces, *Langmuir* **1999**, *15*, 2719-2725.
90. Resch, R.; Baur, C.; Bugacov, A.; Koel, B. E.; Madhukar, A.; Requicha, A. A. G.; Will, P. Building and Manipulating Three-Dimensional and Linked Two-Dimensional

Structures of Nanoparticles Using Scanning Force Microscopy, *Langmuir* **1998**, *14*, 6613-6616.

91. Harel, E.; Meltzer, S. E.; Requicha, A. A. G.; Thompson, M. E.; Koel, B. E. Fabrication of Polystyrene Latex Nanostructures by Nanomanipulation and Thermal Processing, *Nano Lett.* **2005**, *5*, 2624-2629.
92. Postma, H. W. Ch.; Teepen, T.; Yao, Z.; Grifoni, M.; Dekker, C. Carbon Nanotube Single-Electron Transistors at Room Temperature, *Science* **2001**, *293*, 76-79.
93. Hertel, T.; Martel, R.; Avouris, P. Manipulation of Individual Carbon Nanotubes and their Interaction with Surfaces, *J. Phys. Chem. B* **1998**, *102*, 910-915.

CHAPTER 2: DIRECTIONAL ORIENTATION OF CARBON NANOTUBES ON SURFACES USING A GAS FLOW CELL*

2.1 Introduction

Carbon nanotubes (CNTs) have generated significant interest as a nanoscale material because of their structural, mechanical, electronic, and chemical properties. Considerable research effort has been directed toward using CNTs as building blocks in the fabrication of nanometer-sized components in devices such as transistors [1-3], logic gates [4], and sensors [5, 6]. Direct-growth and post-growth approaches have been used to manipulate CNTs in the fabrication of these devices. In direct-growth processes, CNTs are grown from catalyst in the desired positions using chemical vapor deposition (CVD) methods [1, 5, 6], while in post-growth strategies, CNTs are self-assembled using biomolecular recognition [2], manipulated by an atomic force microscope (AFM) tip [3], or directly deposited on surfaces [4]. Other post-growth nanotube alignment approaches that have been reported involve an electric field [7], a magnetic field [8], or surface

---

* This chapter is adapted with permission from *Nano Lett.* **2004**, *4*, 1481-1484. Copyright 2004 American Chemical Society.

chemistry patterned lithographically [9].

To produce large-scale devices, precise control of the orientation and location of CNTs on surfaces is essential. Various strategies have been developed to grow horizontally aligned CNTs in a controlled manner by CVD [10-13]. Several post-growth techniques have also been reported for controlling surface positioning and alignment of CNTs. Microfluidic flow was used to form oriented CNTs on a patterned surface [14], the direction of CNTs was controlled while dispersing them in a nematic liquid crystal [15], and ordered arrays of CNTs were obtained from a flowing sodium dodecyl sulfate-CNT suspension on a silanized substrate [16]. In Chapter 3, I demonstrate the localization of CNTs on aligned surface DNA templates that were coated with 1-pyrenemethylamine, to provide oriented CNTs on substrates [17]. I report here a simple approach that can control the large-scale alignment of CNTs on surfaces, using flowing gas over a droplet of CNT suspension. The orientation of CNTs on the surface is dictated by the direction of the gas flow. Horizontally aligned, parallel CNTs and two-dimensional, orthogonally positioned nanotube networks can be fabricated easily by this technique. I have also investigated the mechanism of CNT alignment on surfaces in the gas flow system.

2.2 Experimental Section

Single-walled carbon nanotube (SWNT) suspensions for surface alignment were prepared as follows. Acid-purified SWNTs (0.2 mg, Carbon Solutions Inc., Riverside, CA) were added to 2 mL *N*,*N*-dimethylformamide (DMF, EM Science, Gibbstown, NJ) and sonicated for 1 h. This concentrated SWNT suspension was diluted with DMF to 0.05 mg/mL and sonicated for one more hour, resulting in SWNT lengths of ~1 μm.

SWNT suspensions prepared in this fashion could be used for several weeks; suspensions prepared more than ~1 month previously tended to resettle and precipitate.

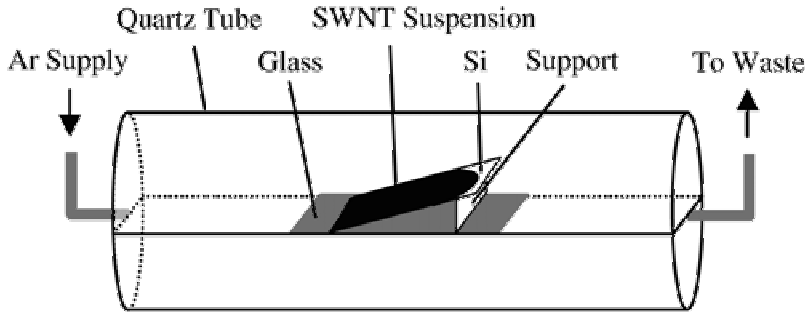

Figure 2.1 Schematic diagram of the gas flow SWNT alignment system.

Si surfaces for SWNT alignment were prepared by immersing a Si wafer (TTI Silicon, Sunnyvale, CA) in 10% HF for 3 min and then thoroughly rinsing with water from a Barnstead purification system (Dubuque, IA). The wafer was cut into ~5 × 8 mm pieces to serve as substrates for SWNT alignment. Each Si substrate was treated with 10 μg/mL aqueous poly-L-lysine solution (Ted Pella, Redding, CA). After 10 min the poly-L-lysine solution was removed, and the surface was rinsed with water and dried with compressed air. A 20 μL droplet of the diluted SWNT suspension was pipetted onto the Si substrate, which was placed on a glass holder and tilted upward at a ~20° angle in the middle of a 2.3-cm diameter quartz tube (Figure 2.1). Ar gas flow was applied through the tube for 10 min at an average linear velocity of 6-9 cm/s. After flow was stopped and the substrate was removed from the tube, the SWNT suspension was pipetted off, and the Si substrate was rinsed with DMF followed by water and then dried with compressed air. On some surfaces, I did a second SWNT alignment step to create orthogonal nanotube arrays. To make these surfaces, after the first SWNT alignment step the substrate had another 20 μL droplet of SWNT suspension placed atop it. Then, the silicon piece was

placed into the flow cell rotated ~90° from its arrangement for the initial alignment, and the gas flow and rinsing steps were carried out as described above.

Control surfaces were prepared identically to aligned samples, except no Ar gas was flowed through the quartz tube.

2.3 Results and Discussion

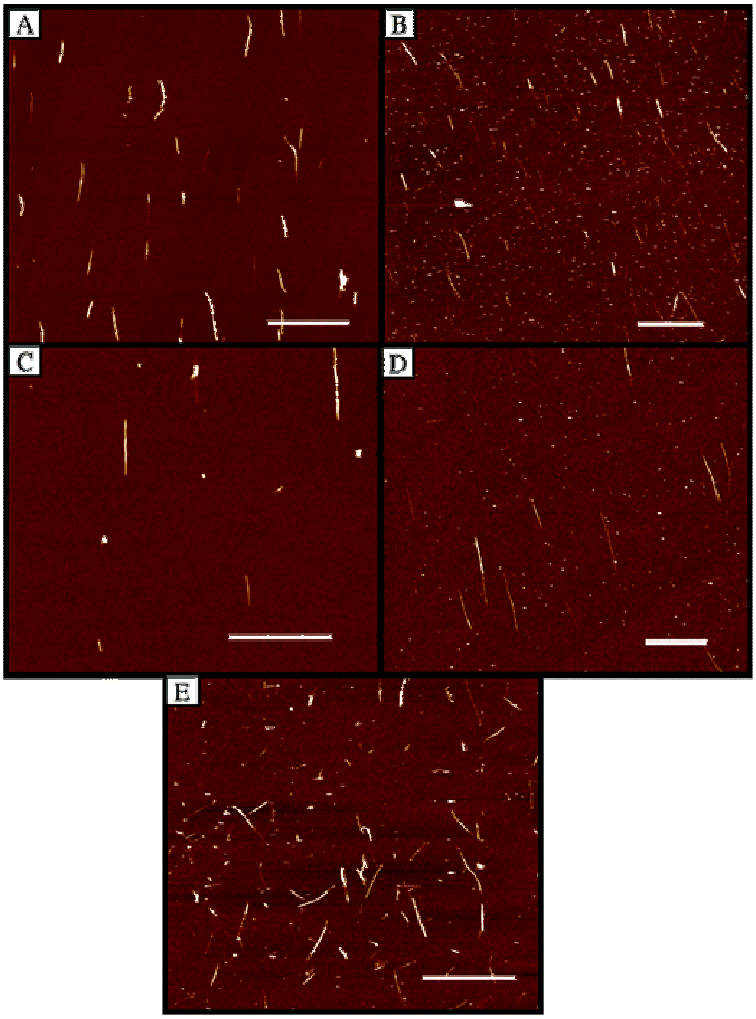

Figure 2.2 Typical AFM height images of aligned SWNTs on two different substrates, along with a control surface having randomly oriented SWNTs. (A) and (B) are larger-area images of aligned nanotube substrates; (C) and (D) are smaller-area images of SWNTs aligned on surfaces; and (E) is an image of a control surface, which was not subjected to the gas flow alignment protocol. The height scale is 12 nm in (A-D) and 8 nm in (E). The scale bars indicate 2.5 µm in (A) and (E), 5 µm in (B), and 1 µm in (C) and (D).

All substrates were analyzed by AFM [18]; images of prepared samples show that most SWNTs are aligned in the direction of the Ar flow, as seen in Figure 2.2A-D. For three different substrates I analyzed, obtaining ten AFM images from each surface, the SWNT angular orientation distributions are shown in Figure 2.3A-C. The distribution patterns on the three substrates are all similar. I also observed no statistically significant difference in angular orientation profiles between individual SWNTs (<2 nm AFM height) and SWNT bundles (2-10 nm AFM height) on aligned surfaces. Based on data from these samples, I conclude that on average, 74% of SWNTs are distributed within a ±5° angular spread relative to the gas flow direction, and 85% of SWNTs are within a ±10° angular spread. In contrast, on control substrates prepared in the absence of gas flow the orientations of SWNTs are distributed randomly across the entire angular range (Figures 2.2E and 2.3D). A second orthogonal alignment of SWNT suspension led to approximately perpendicular SWNT orientations on surfaces (Figure

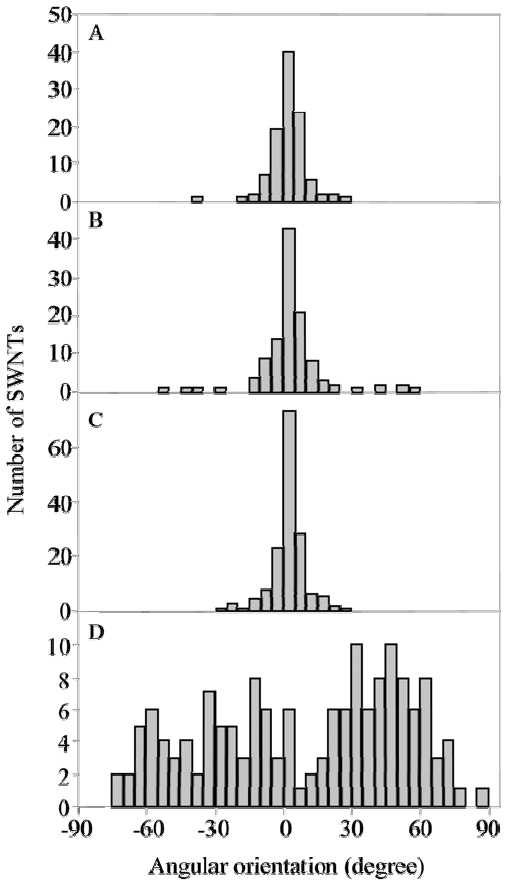

Figure 2.3 SWNT angular orientation distributions. (A-C) Three different surfaces where SWNT suspensions were aligned on substrates in the gas flow cell. (D) Control sample prepared identically to those in (A-C), except there was no gas flow in the alignment system.

2.4). I have also studied the alignment of longer SWNT samples and found that SWNTs with lengths up to 10 µm can be oriented on surfaces using this approach.

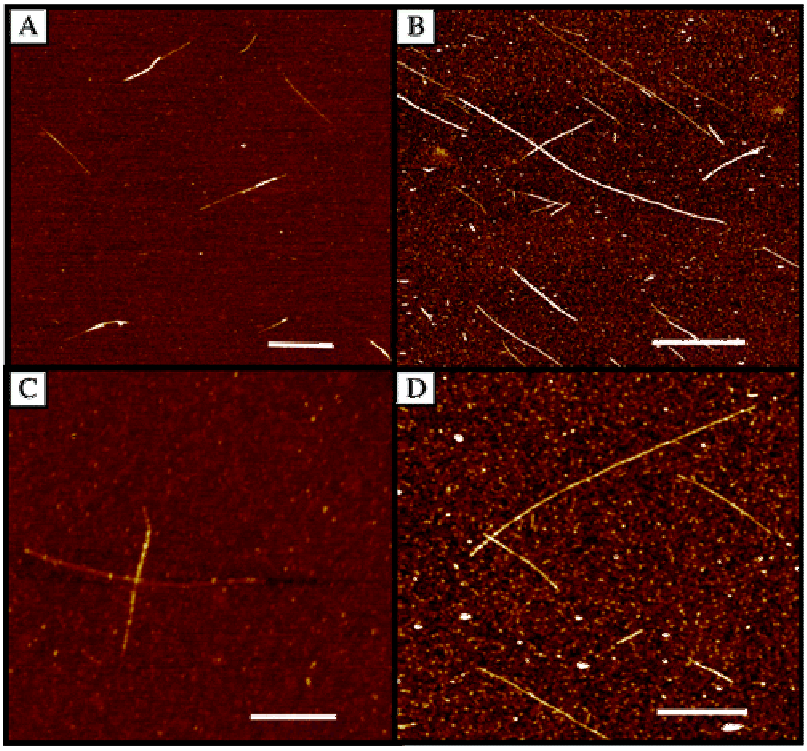

Figure 2.4 AFM height images of perpendicularly aligned SWNTs on two different substrates. (A) and (B) are larger-area images, while (C) and (D) are smaller-area images. The height scales are 12, 6, 15, and 6 nm for (A), (B), (C), and (D), respectively. The scale bars indicate 1 µm in (A) and (B), and 500 nm in (C) and (D).

When I designed this alignment system, my initial expectation was that the droplet of SWNT suspension would move across the substrate under the influence of the Ar flow, which would align SWNTs on the surface [16] in a manner similar to earlier work where DNA was aligned on surfaces [19]. However, upon visual inspection I did not observe motion of the entire SWNT suspension droplet in the flow cell. Thus, to understand the mechanism of SWNT alignment under gas flow on surfaces using this system, I monitored the motion of SWNT precipitates within a droplet on a surface as a function of time, using a >1 month old SWNT suspension that had begun to precipitate. A

20 μL portion of this partially precipitated SWNT suspension was pipetted onto a Si substrate, the surface was placed in the gas flow system, and a series of continuous pictures was taken with a 6 s interval between images using a Coolpix995 digital camera (Nikon, Tokyo, Japan). Precipitates moved in an approximately oval path around the SWNT suspension droplet; moreover, the distances traveled between pictures by different precipitates were not the same, indicating different velocities (Figure 2.5).

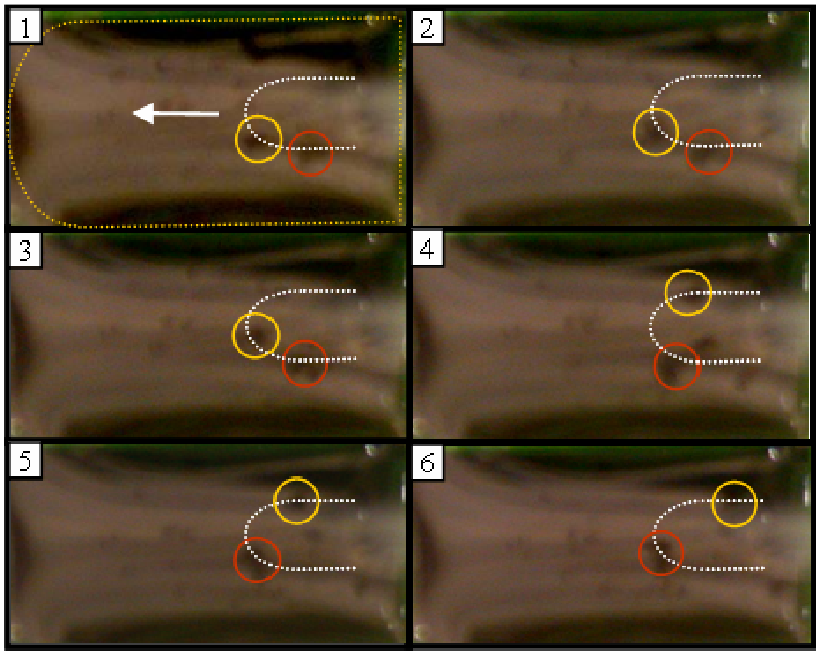

Figure 2.5 A series of digital images taken of SWNT precipitates in DMF, showing fluid circulation within a droplet in the gas flow system. The time interval between pictures is 6 s. The dashed yellow line surrounds the DMF droplet, and the white arrow depicts the Ar flow direction in (1). The dotted, white half-ovals indicate the approximate movement path of the precipitates. The yellow and red circles in each image show the locations of two separate SWNT precipitates.

I observed several types of fluid circulation in droplets [20] in the flow cell: clockwise, counterclockwise, and recirculation involving both clockwise and counterclockwise motion (Figure 2.6). Importantly, the movement of SWNT precipitates was observed only while the gas flow occurred; both before and after the application of Ar flow, all precipitates remained static. These results clearly show that the gas flow

leads to fluid circulation within the droplet. A closer inspection of precipitates moving with different velocities indicated that smaller-sized precipitates had faster speeds and moved greater distances along the substrate than larger-sized ones. Based on these observations, I believe that circulation velocities and trajectories within droplets are dependent on the mass and size of suspended particles or precipitates. Furthermore, I observed in AFM images that SWNTs on surfaces were not aligned when the average linear Ar flow rate was below 6 cm/s, which indicates that the gas flow rate is an important factor in achieving SWNT alignment.

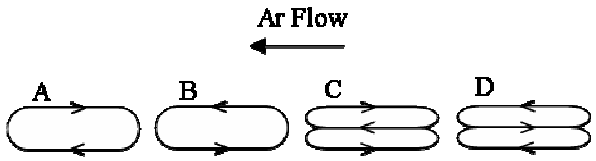

Figure 2.6 Top view of four typical types of circulation in droplets in the gas flow cell. (A) Clockwise; (B) counter-clockwise; (C) and (D) recirculation involving clockwise and counterclockwise motion. Circulation in Figure 2.5 is of the type shown in (A).

From these experiments, I infer that (1) because of their smaller sizes, individual SWNTs or SWNT bundles in suspension move faster than the aggregated precipitates under Ar flow; (2) SWNTs in suspension move across the entire substrate length, because AFM images taken from various regions spanning the substrate show aligned SWNTs; and (3) the circulation of SWNTs in suspension within the droplet, combined with the attraction between the amine groups in poly-L-lysine and the SWNT sidewalls [21], leads to the deposition of aligned SWNTs on the surface. The necessity of the poly-L-lysine surface treatment was further verified on a control substrate, which was not modified with this reagent; importantly, no SWNTs were observed on this surface.

2.4 Conclusions

In summary, I have presented a simple method that enables facile control of the orientation of SWNTs over the entire area of several-millimeter-scale Si surfaces. Two-dimensional orthogonal SWNT arrangements can also be achieved using this approach in a two-step process. This post-growth SWNT manipulation technique should be a valuable tool in the fabrication of devices with aligned SWNTs. In particular, the ability to increase the relative concentration of SWNTs with a given angular orientation may be advantageous for improving yields in the bottom-up assembly of biologically or chemically templated nanotube nanodevices, such as those developed in Chapters 3-5.

2.5 References

1. Li, S.; Yu, Z.; Yen, S.-F.; Tang, W. C.; Burke, P. J. Carbon Nanotube Transistor Operation at 2.6 GHz, *Nano Lett.* **2004**, *4*, 753-756.
2. Keren, K.; Berman, R. S.; Buchstab, E.; Sivan, U.; Braun, E. DNA-Templated Carbon Nanotube Field-Effect Transistor, *Science* **2003**, *302*, 1380-1382.
3. Postma, H. W. Ch.; Teepen, T.; Yao, Z.; Grifoni, M.; Dekker, C. Carbon Nanotube Single-Electron Transistors at Room Temperature, *Science* **2001**, *293*, 76-79.
4. Derycke, V.; Martel, R.; Appenzeller, J.; Avouris, Ph. Carbon Nanotube Inter- and Intramolecular Logic Gates, *Nano Lett.* **2001**, *1*, 453-456.
5. Qi, P.; Vermesh, O.; Grecu, M.; Javey, A.; Wang, Q.; Dai, H.; Peng, S.; Cho, K. J. Toward Large Arrays of Multiplex Functionalized Carbon Nanotube Sensors for Highly Sensitive and Selective Molecular Detection, *Nano Lett.* **2003**, *3*, 347-351.
6. Lin, Y.; Lu, F.; Tu, Y.; Ren, Z. Glucose Biosensors Based on Carbon Nanotube Nanoelectrode Ensembles, *Nano Lett.* **2004**, *4*, 191-195.
7. Nagahara, L. A.; Amlani, I.; Lewenstein, J.; Tsui, R. K. Directed Placement of Suspended Carbon Nanotubes for Nanometer-Scale Assembly, *Appl. Phys. Lett.* **2002**, *80*, 3826-3828.
8. Walters, D. A.; Casavant, M. J.; Qin, X. C.; Huffman, C. B.; Boul, P. J.; Ericson, L. M.; Haroz, E. H.; O'Connell, M. J.; Smith, K.; Colbert, D. T.; Smalley, R. E. In-Plane-Aligned Membranes of Carbon Nanotubes, *Chem. Phys. Lett*. **2001**, *338*, 14-20.
9. Choi, K. H.; Bourgoin, J. P.; Auvray, S.; Esteve, D.; Duesberg, G. S.; Roth, S.; Burghard, M. Controlled Deposition of Carbon Nanotubes on a Patterned Substrate, *Surf. Sci.* **2000**, *462*, 195-202.

10. Huang, L.; Wind, S. J.; O'Brien, S. P. Controlled Growth of Single-Walled Carbon Nanotubes from an Ordered Mesoporous Silica Template, *Nano Lett*. **2003**, *3*, 299-303.

11. Zhang, Y.; Chang, A.; Cao, J.; Wang, Q.; Kim, W.; Li, Y.; Morris, N.; Yenilmez, E.; Kong, J.; Dai, H. Electric-Field-Directed Growth of Aligned Single-Walled Carbon Nanotubes, *Appl. Phys. Lett.* **2001**, *79*, 3155-3157.

12. Huang, S.; Cai, X.; Liu, J. Growth of Millimeter-Long and Horizontally Aligned Single-Walled Carbon Nanotubes on Flat Substrates, *J. Am. Chem. Soc.* **2003**, *125*, 5636-5637.

13. Joselevich, E.; Lieber, C. M. Vectorial Growth of Metallic and Semiconducting Single-Wall Carbon Nanotubes, *Nano Lett.* **2002**, *2*, 1137-1141.

14. Ko, H.; Peleshanko, S.; Tsukruk, V. V. Combing and Bending of Carbon Nanotube Arrays with Confined Microfluidic Flow on Patterned Surfaces, *J. Phys. Chem. B* **2004**, *108*, 4385-4393.

15. Lynch, M. D.; Patrick, D. L. Organizing Carbon Nanotubes with Liquid Crystals, *Nano Lett.* **2002**, *2*, 1197-1201.

16. Lay, M. D.; Novak, J. P.; Snow, E. S. Simple Route to Large-Scale Ordered Arrays of Liquid-Deposited Carbon Nanotubes, *Nano Lett*. **2004**, *4*, 603-606.

17. Xin, H.; Woolley, A. T. DNA-Templated Nanotube Localization, *J. Am. Chem. Soc.* **2003**, *125,* 8710-8711.

18. Images were obtained with a Multimode IIIa AFM instrument (Veeco, Sunnyvale, CA) using microfabricated, aluminum-coated silicon cantilever tips (Nanoscience Instruments, Phoenix, AZ). Vibrational noise was minimized with an active isolation

system (MOD1-M, Halcyonics, Goettingen, Germany). Typical imaging parameters were: tip resonance frequency, 55-65 kHz; free oscillation amplitude, 0.9-1.1 V; setpoint, 0.4-0.7 V; scan rate, 1.6 Hz. Images were processed offline to remove background curvature using software bundled with the AFM instrument.

19. Woolley, A. T.; Kelly, R. T. Deposition and Characterization of Extended Single-Stranded DNA Molecules on Surfaces, *Nano Lett.* **2001**, *1*, 345-348.
20. LeClair, B. P.; Hamielec, A. E.; Pruppacher, H. R.; Hall, W. D. A Theoretical and Experimental Study of the Internal Circulation in Water Drops Falling at Terminal Velocity in Air, *J. Atmos. Sci.* **1972**, 29, 728-740.
21. Liu, J.; Casavant, M. J.; Cox, M.; Walters, D. A.; Boul, P.; Lu, W.; Rimberg, A. J.; Smith, K. A.; Colbert, D. T.; Smalley, R. E. Controlled Deposition of Individual Single-Walled Carbon Nanotubes on Chemically Functionalized Templates, *Chem. Phys. Lett.* **1999**, *303*, 125-129.

CHAPTER 3: DNA-TEMPLATED NANOTUBE LOCALIZATION*

3.1 Introduction

The construction and evaluation of materials and devices with nanometer dimensions has become an area of rapidly expanding research interest. Carbon nanotubes have emerged as important materials for nanofabrication, in both electronic devices [1-3] and sensors [4-8]. A key issue in the use of carbon nanotubes in nanofabrication is the need for their controlled placement at well-defined positions on surfaces. Previous efforts to control localization of nanotubes or nanorods have included the use of microfluidics [9,10], an applied electric field [11,12], or patterning using side edges of multilayer films [13,14]. An intriguing approach for assembly of nanoscale materials is the use of a biological template to direct the positioning of components on a surface. DNA is an attractive candidate template, since it possesses a small diameter (~2 nm), controllable length that can exceed 10 μm, and the ability to use molecular recognition in forming specific base pairs. Indeed, recent work has demonstrated the application of DNA in

---

* This chapter is adapted with permission from *J. Am. Chem. Soc.* **2003**, *125*, 8710-8711.

construction of various types of metallic nanowires [15-20]. In this work, I report a novel method that enables selective localization of single-walled carbon nanotubes (SWNTs) on aligned DNA molecules on surfaces. This approach represents a simple route to manipulation and positioning of SWNTs on surfaces, and provides an important tool in bottom-up biotemplated nanofabrication.

3.2 Experimental Section

My approach for directed placement of SWNTs on surfaces involves aligning DNA on a substrate, treating the surface with a bifunctional bridging compound, and then exposing the substrate to a SWNT suspension. Double-stranded λ DNA was linearly aligned on a Si surface that had been treated with 1 ppm aqueous poly-L-lysine, following a previously developed method [21]. Next, the Si with aligned DNA was submerged in a 6 mM solution of 1-pyrenemethylamine hydrochloride (PMA) (Aldrich, Milwaukee, WI) in *N*,*N*-dimethylformamide (DMF) (EM Science, Gibbstown, NJ) for 12 h in the dark. Finally, a 40 μL droplet of a 0.1 mg/mL acid-purified SWNT (Carbon Solutions Inc., Riverside, CA) suspension in DMF [22] was pipetted onto the Si substrate and allowed to sit for 20 min. Between each step, the substrates were rinsed thoroughly with deionized water, or with both DMF and water, and dried under a stream of compressed air. In a control experiment, I directly exposed a Si substrate with aligned DNA to the SWNT suspension, without the PMA treatment step.

3.3 Results and Discussion

Figure 3.1 shows an atomic force microscopy (AFM) height image of λ DNA aligned on a Si surface and treated with PMA; for comparison, the inset depicts a surface with aligned λ DNA not exposed to PMA [23]. Round elevated features along the DNA are indicative of clusters of PMA that decorate the DNA; in addition, a small amount of nonspecific deposition of PMA clusters is observed on the Si surface [24]. The amine group in PMA is expected to interact electrostatically with the negatively charged phosphate backbone of DNA, while the aromatic pyrenyl group is known to interact strongly with the surfaces of SWNTs through π-stacking forces [25]. Thus, the localization of PMA primarily on the DNA should enable the specific assembly of SWNTs on surface DNA molecules.

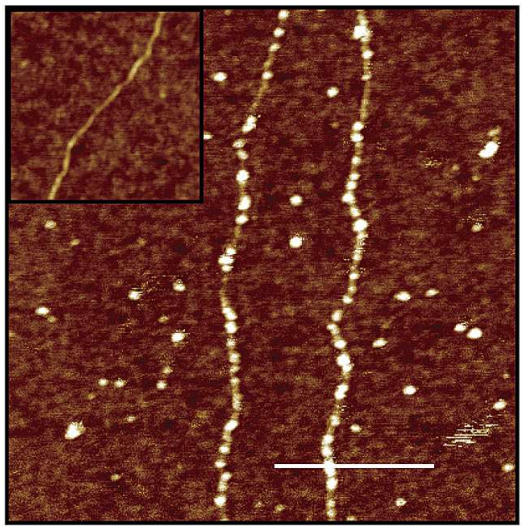

Figure 3.1 AFM height images of untreated (inset) and PMA-treated λ DNA aligned on a Si surface. The height scale is 6 nm, and the white bar indicates 250 nm.

I used AFM to image three different Si substrates that had SWNTs deposited onto PMA-treated, aligned DNA. I obtained 60 images on these substrates, covering an area of ~600 μm^2 on each surface. Representative AFM images from these surfaces are shown in Figure 3.2. All three images show aligned DNA and one or more SWNTs specifically localized on the nucleic acid template. Nanotube heights range from 1.3 to 9 nm, suggesting that a mixture of SWNT bundles and individual SWNTs has been deposited.

From the 60 AFM images on all three substrates, I determined that 63% of SWNTs observed on the surface were anchored along DNA, while the DNA itself covered only ~1% of the surface area. The lack of perfect selectivity in SWNT placement can be explained in part by the presence of some nonspecifically deposited PMA on the surfaces. Importantly, on a control substrate where the DNA was not treated with PMA, only ~10% of the SWNTs were aligned on DNA; these results suggest that PMA plays a key role in the selectivity of SWNT deposition onto surface DNA.

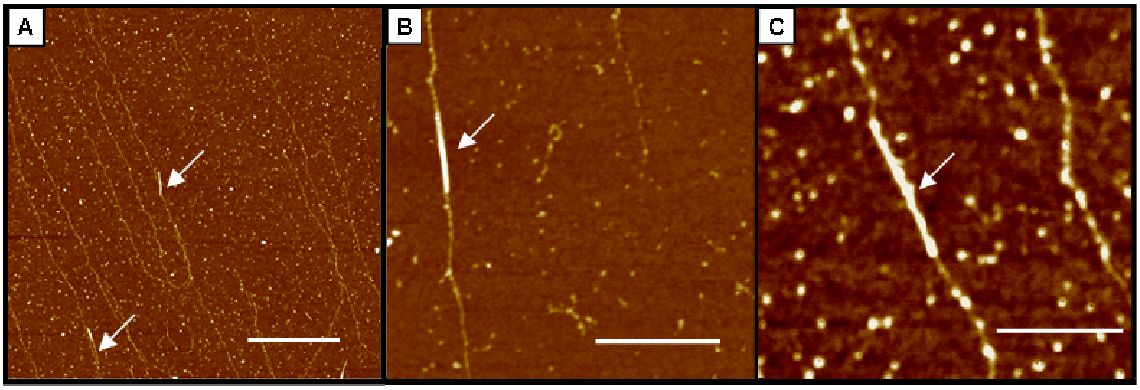

Figure 3.2 AFM height images of λ DNA-templated SWNT positioning on Si surfaces. (A) Large area image of SWNTs deposited on PMA-treated DNA. White arrows indicate SWNTs; height scale is 12 nm, and the white bar indicates 1000 nm. (B,C) Smaller area images of two different substrates where SWNTs were deposited onto PMA-treated DNA. White arrows indicate SWNTs. The height scale is 18 nm and the white bar indicates 500 nm in (B), while the height scale is 4 nm and the white bar indicates 250 nm in (C).

The AFM data in Figure 3.2 indicate incomplete coverage of the surface DNA with SWNTs. In 12 typical images, I measured the total length of all surface DNA, as well as the total length of specifically deposited SWNTs. From these measurements I determined that, on average, ~5% of the total DNA length was covered with specifically aligned SWNTs. I attribute the partial coverage to three factors. First, stable SWNT suspensions could be made only at concentrations ≤0.1 mg/mL, which limited the total number of SWNTs available for localization on surface DNA. Suspensions with higher

SWNT concentrations tended to aggregate and precipitate. Second, in the suspension, only SWNTs that are nearly parallel with aligned DNA have a strong interaction with the PMA/DNA complex, because the local concentration of PMA is higher along the DNA than on the rest of the Si surface. For SWNTs with other orientations, the interaction usually is not strong enough to align SWNTs specifically on DNA. Finally, because DNA-templated SWNT assembly occurs only at the surface, the number of SWNTs available for binding to DNA is constrained by the diffusion rate of SWNTs through the bulk solution. Utilizing recent advances in SWNT solubilization [25, 26] should increase the number of SWNTs in solution and address the first limitation, while the use of active mixing during deposition should help to overcome the latter two constraints.

3.4 Conclusions

In conclusion, I have developed a technique to specifically localize SWNTs onto PMA-decorated λ DNA molecules aligned on Si surfaces. With this method, over 60% of all SWNTs deposited on substrates are aligned on DNA fragments. This approach offers significant potential to facilitate the construction of ordered arrays of nanometer dimension materials. Finally, combining DNA-templated nanotube localization with the ability to form specific base pairs between oligonucleotide coupled nanostructures and surface DNA may enable the bottom-up construction of nanoscale electronic circuits.

3.5 References

1. Collins, P. G.; Zettl, A.; Bando, H.; Thess, A.; Smalley, R. E. Nanotube Nanodevice, *Science* **1997**, *278*, 100-103.
2. Tans, S. J.; Devoret, M. H.; Dai, H. J.; Thess, A.; Smalley, R. E.; Geerligs, L. J.; Dekker, C. Individual Single-Wall Carbon Nanotubes as Quantum Wires, *Nature* **1997**, *386*, 474-477.
3. Shim, M.; Javey, A.; Kam, N. W. S.; Dai, H. Polymer Functionalization for Air-Stable n-Type Carbon Nanotube Field-Effect Transistors, *J. Am. Chem. Soc.* **2001**, *123*, 11512-11513.
4. Kong, J.; Franklin, N. R.; Zhou, C. W.; Chapline, M. G.; Peng, S.; Cho, K. J.; Dai, H. Nanotube Molecular Wires as Chemical Sensors, *Science* **2000**, *287*, 622-625.
5. Varghese, O. K.; Kichambre, P. D.; Gong, D.; Ong, K. G.; Dickey, E. C.; Grimes, C. A. Gas Sensing Characteristics of Multi-Wall Carbon Nanotubes, *Sens. Actuators B* **2001**, *81*, 32-41.
6. Chopra, S.; Pham, A.; Gaillard, J.; Parker, A.; Rao, A. M. Carbon-Nanotube-Based Resonant-Circuit Sensor for Ammonia, *Appl. Phys. Lett.* **2002**, *80*, 4632-4634.
7. Qi, P.; Vermesh, O.; Grecu, M.; Javey, A.; Wang, Q.; Dai, H.; Peng, S.; Cho, K. J. Toward Large Arrays of Multiplex Functionalized Carbon Nanotube Sensors for Highly Sensitive and Selective Molecular Detection, *Nano Lett.* **2003**, *3*, 347-351.
8. Valentini, L.; Armentano, I.; Kenny, J. M.; Cantalini, C.; Lozzi, L.; Santucci, S. Sensors for Sub-ppm NO_2 Gas Detection Based on Carbon Nanotube Thin Films, *Appl. Phys. Lett.* **2003**, *82*, 961-963.
9. Messer, B.; Song, J. H.; Yang, P. D. Microchannel Networks for Nanowire Patterning,

J. Am. Chem. Soc. **2000**, *122*, 10232-10233.

10. Cui, Y.; Lieber, C. M. Functional Nanoscale Electronic Devices Assembled Using Silicon Nanowire Building Blocks, *Science* **2001**, *291*, 851-853.
11. Joselevich, E.; Lieber, C. M. Vectorial Growth of Metallic and Semiconducting Single-Wall Carbon Nanotubes, *Nano Lett.* **2002**, *2*, 1137-1141.
12. Nagahara, L. A.; Amlani, I.; Lewenstein, J.; Tsui, R. K. Directed Placement of Suspended Carbon Nanotubes for Nanometer-Scale Assembly, *Appl. Phys. Lett.* **2002**, *80*, 3826-3828.
13. Melosh, N. A.; Boukai, A.; Diana, F.; Gerardot, B.; Badolato, A.; Petroff, P. M.; Heath, J. R. Ultrahigh-Density Nanowire Lattices and Circuits, *Science* **2003**, *300*, 112-115.
14. Artemyev, M.; Moller, B.; Woggon, U. Unidirectional Alignment of CdSe Nanorods, *Nano Lett.* **2003**, *3*, 509-512.
15. Braun, E.; Eichen, Y.; Sivan, U.; Ben-Yoseph, G. DNA-Templated Aassembly and Electrode Attachment of a Conducting Silver Wire, *Nature* **1998**, *391*, 775-778.
16. Richter, J.; Mertig, M.; Pompe, W.; Mönch, I.; Schackert, H. K. Construction of Highly Conductive Nanowires on a DNA Template, *Appl. Phys. Lett.* **2001**, *78*, 536-538.
17. Ford, W. E.; Harnack, O.; Yasuda, A.; Wessels, J. M. Platinated DNA as Precursors to Templated Chains of Metal Nanoparticles, *Adv. Mater.* **2001**, *13*, 1793-1797.
18. Patolsky, F.; Weizmann, Y.; Lioubashevski, O.; Willner, I. Au Nanoparticle Nanowires Based on DNA and Polylysine Templates, *Angew. Chem., Int. Ed.* **2002**, *41*, 2323-2327.

19. Keren, K.; Kreuger, M.; Gilad, R.; Ben-Yoseph, G.; Sivan, U.; Braun, E. Sequence-Specific Molecular Lithography on Single DNA Molecules, *Science* **2002**, *297*, 72-75.

20. Monson, C. F.; Woolley, A. T. DNA-Templated Construction of Copper Nanowires, *Nano Lett.* **2003**, *3*, 359-363.

21. Woolley, A. T.; Kelly, R. T. Deposition and Characterization of Extended Single-Stranded DNA Molecules on Surfaces, *Nano Lett.* **2001**, *1*, 345-348.

22. The SWNT suspension was prepared by sonicating 0.4 mg of SWNTs in 4 mL of DMF for 20 h in an ultrasonic bath.

23. Images were obtained with a Multimode IIIa AFM instrument with microfabricated Si cantilever tips (Veeco, Sunnyvale, CA). Vibrational noise was minimized using an active isolation system (MOD1-M, Halcyonics, Goettingen, Germany). Typical imaging parameters were (a) tip resonance frequency, 55-65 kHz; (b) free oscillation amplitude, 0.9-1.1 V; (c) setpoint, 0.4-0.7 V; (d) scan rate, 1.2-1.6 Hz. Images were processed offline to remove the background slope using software bundled with the AFM instrument.

24. The average height of the PMA features on the DNA exceeds that of the underlying DNA by 1.5 nm, while the nonspecifically deposited PMA features extend 2.6 nm (on average) above the surface. Since the molecular dimension of PMA on its longest axis is <1.0 nm, the heights of the elevated round features in Figure 1 are consistent with PMA clusters rather than individual molecules.

25. Chen, R. J.; Zhang, Y.; Wang, D.; Dai, H. Noncovalent Sidewall Functionalization of Single-Walled Carbon Nanotubes for Protein Immobilization, *J. Am. Chem. Soc.*

2001, *123*, 3838-3839.

26. Star, A.; Steuerman, D. W.; Heath, J. R.; Stoddart, J. F. Starched Carbon Nanotubes, *Angew. Chem., Int. Ed.* **2002**, *41*, 2508-2512.

CHAPTER 4: HIGH-YIELD DNA-TEMPLATED ASSEMBLY OF SURFACTANT-WRAPPED CARBON NANOTUBES*

4.1 Introduction

The miniaturization of electronic circuits to have feature sizes reaching nanometer dimensions has become an attractive research area, because of numerous potential device applications in diverse fields, including automotive products, information technology, and biomedical sensors [1]. Heavily used top-down fabrication methodologies, which apply photolithographic patterning and etching techniques, continue to make incremental feature size reductions, but with increasing costs. On the other hand, bottom-up fabrication strategies, which build up larger structures from atomic or molecular components, are emerging as an appealing alternative approach, because of potential benefits including low cost [2] and the availability of various building block materials [1].

DNA has highly specific recognition and self-assembly properties, and can be designed and synthesized with desired sequences, making it an attractive template

---

* This chapter is adapted with permission from *Nanotechnology* **2005**, *16*, 2238-2241.

material for bottom-up nanofabrication. Because DNA molecules have a diameter of ~2 nm, but can have lengths exceeding tens of micrometers, they are desirable bottom-up templates for making nanowires. Various metals, including silver [3, 4], palladium [5], platinum [6], gold [7, 8], and copper [4, 9], have been deposited on DNA templates to construct one dimensional nanostructures. In addition, methods have been developed for localizing single-walled carbon nanotubes (SWNTs) on elongated DNA molecules [8, 10].

SWNTs, with their high aspect ratios and unique mechanical and electronic properties, are novel nanofabrication materials. Devices based on SWNTs have been reported as chemical sensors [11, 12] and electronic circuits, including field-effect transistors [8], diodes [13], rectifiers [14], and logic gates [15]. Two approaches have been applied for making arrays of SWNTs on surfaces: *in situ* growth from patterned catalysts [11, 12] or depositing SWNTs from liquid suspensions [8, 15]. While it is feasible to disperse SWNTs in organic solvents [16, 17], for many applications it is desirable to have SWNTs suspended in water. Several methods, including SWNT functionalization with hydrophilic groups [18], wrapping in polymers [19] or single-stranded DNA [20], and solubilization with various surfactants [21, 22], now allow SWNT manipulations in aqueous media. The role of surfactants in the dispersion of SWNTs in aqueous solution has been explored [23-26], and the mechanism of solubilization is believed to involve the encasement of individual SWNTs or small SWNT bundles in cylindrical micelle-like structures, which have the hydrophobic tail groups oriented toward the SWNT sidewalls and the hydrophilic head groups extending into the solution [23, 24].

Both DNA and SWNTs are high-aspect-ratio materials with excellent nanofabrication potential. Recent research combining these two moieties has involved the covalent attachment of DNA oligonucleotides to SWNTs [27, 28], the wrapping of single-stranded DNA around SWNTs to form DNA/SWNT hybrids [20, 29], the self-assembling of oligonucleotide-coupled carbon nanotubes through DNA hybridization [30], and the directed localization of SWNTs on DNA templates [8, 10].

I am interested in utilizing DNA as a template for the localization of continuous SWNT assemblies, which can then serve as nanotube nanowires in nanoelectronic circuits [31]. The diameters of these nanotube nanowires can be <10 nm, the approximate cross-sectional dimension of small SWNT bundles or individual SWNTs; such features would be considerably narrower than current DNA-templated metal nanowires (30-50 nm) [3, 5, 7]. Previously, I described a technique for depositing SWNTs on DNA templates by using 1-pyrenemethylamine as a bridging compound [10]. While this initial method showed selective SWNT placement on DNA, the extent of DNA coverage was only ~5%. In this work, I report a greatly improved approach for constructing SWNT assemblies on DNA templates, which provides greater than an order of magnitude improvement in DNA coverage with SWNTs. In this new method, I disperse SWNTs in aqueous dodecyltrimethylammonium bromide (DTAB), a cationic surfactant, which encases SWNTs in cylindrical micelle-like structures and enables their localization on surface DNA through electrostatic interactions. I have explored the coverage of DNA with SWNTs as a function of SWNT concentration and the number of treatments. Importantly, I have obtained nearly continuous SWNT assemblies under optimized conditions. This

approach should have potential applications in the fabrication of nanoelectronic circuits with SWNTs.

4.2 Experimental Section

4.2.1 Solution Preparation

I used DTAB (Sigma) to suspend SWNTs (Sigma) in aqueous solution. SWNTs were added to 10 mM Tris, 1 mM EDTA, pH 8.0 (TE) buffer containing 1% DTAB and sonicated for 24 h. This suspension was centrifuged for 15 min at 14,000 rpm to remove unsuspended SWNTs. The supernatant (containing DTAB-wrapped SWNTs) was decanted; this suspension appeared dark and was stable for several weeks. Freshly prepared SWNT suspension was diluted fourfold with TE buffer for experiments where lower concentrations of SWNTs were desired.

4.2.2 Surface Preparation

For DNA surface preparation, a ~5 mm × 8 mm Si substrate (TTI Silicon, Sunnyvale, CA) was treated with 40 μL of 1 μg/mL aqueous poly-L-lysine solution for 5 min. Next, the surface was rinsed with water and dried with compressed air. A 1 μL droplet of double-stranded λ DNA solution (3 μg/mL in TE buffer) was translated across the surface to elongate the DNA, following a previously developed method [32]. Then, a 40 μL aliquot of the SWNT suspension was pipetted onto the Si surface, and after 10 min the surface was rinsed with water and dried with compressed air. For experiments studying the effects of multiple treatments, a series of surfaces with aligned DNA were exposed to SWNT suspension one to six times.

4.2.3 Imaging Conditions

All substrates were studied by atomic force microscopy (AFM). Images were taken with a Multimode IIIa AFM setup (Veeco, Sunnyvale, CA) using aluminium-coated silicon tips (Nanoscience Instruments, Phoenix, AZ). Vibrational noise was damped with an active isolation system (MOD1-M, Halcyonics, Goettingen, Germany). AFM imaging parameters were as follows: tip resonance frequency, 55-65 kHz; free oscillation amplitude, 0.9-1.1 V; set-point, 0.4-0.7 V; scan rate, 0.8-1.6 Hz. Images were processed after acquisition to eliminate background curvature.

4.3 Results and Discussion

4.3.1 DNA-SWNT Interaction

I hypothesized that the DTAB-wrapped SWNTs would localize on the surface DNA, due to electrostatic interactions between the negatively charged DNA phosphate groups and the positively charged DTAB head groups, as shown in Figure 4.1. To investigate the extent and specificity of the placement of DTAB-wrapped SWNTs on DNA, I analyzed AFM images of DNA surfaces treated with SWNTs. AFM measurements of surface-deposited, DTAB-wrapped

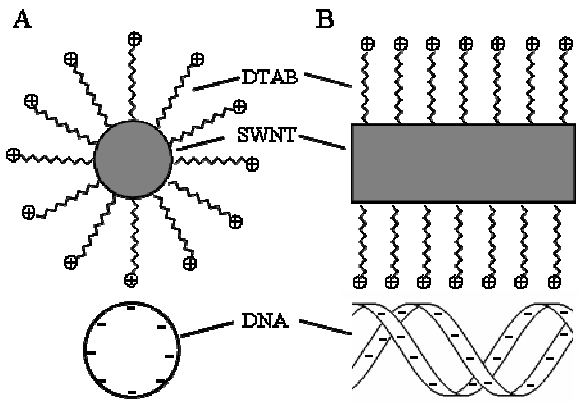

Figure 4.1 Schematic diagram of DTAB-wrapped SWNT localization on DNA. (A) Cross-sectional view; (B) side view.

SWNTs revealed heights of 1.4-7.5 nm, indicating that a mixture of individual SWNTs and small SWNT bundles was deposited. From the AFM images, I also determined two key parameters: DNA coverage and localization selectivity. I define DNA coverage to be the percentage given by dividing the sum of the lengths of all SWNTs localized on DNA by the sum of the lengths of all DNA molecules in a given AFM image. The localization selectivity is the percentage obtained by dividing the sum of the lengths of all SWNTs deposited on DNA by the sum of the lengths of all SWNTs in an AFM image. For each type of surface, the DNA coverage and localization selectivity were averaged from 30-50 AFM images on a minimum of three substrates.

4.3.2 SWNT Deposition from Dilute Solutions

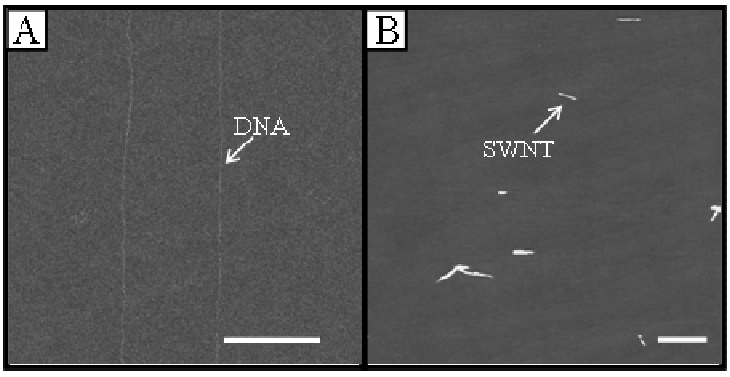

Figure 4.2 AFM height images of control surfaces (A) having only aligned λ DNA and (B) lacking aligned DNA, but treated once with DTAB-wrapped SWNTs. The height scale is 5 nm, and the white bars indicate 1 μm in both images.

The results of control experiments to confirm the DNA-specific alignment of SWNTs on surfaces are presented in Figure 4.2. An AFM image of a substrate having only aligned λ DNA is shown in Figure 4.2A; the average DNA height was 0.8 nm. In Figure 4.2B, DTAB-wrapped SWNTs were deposited on a surface that lacked DNA; the nanotubes are oriented in various directions and have heights that are twofold to tenfold

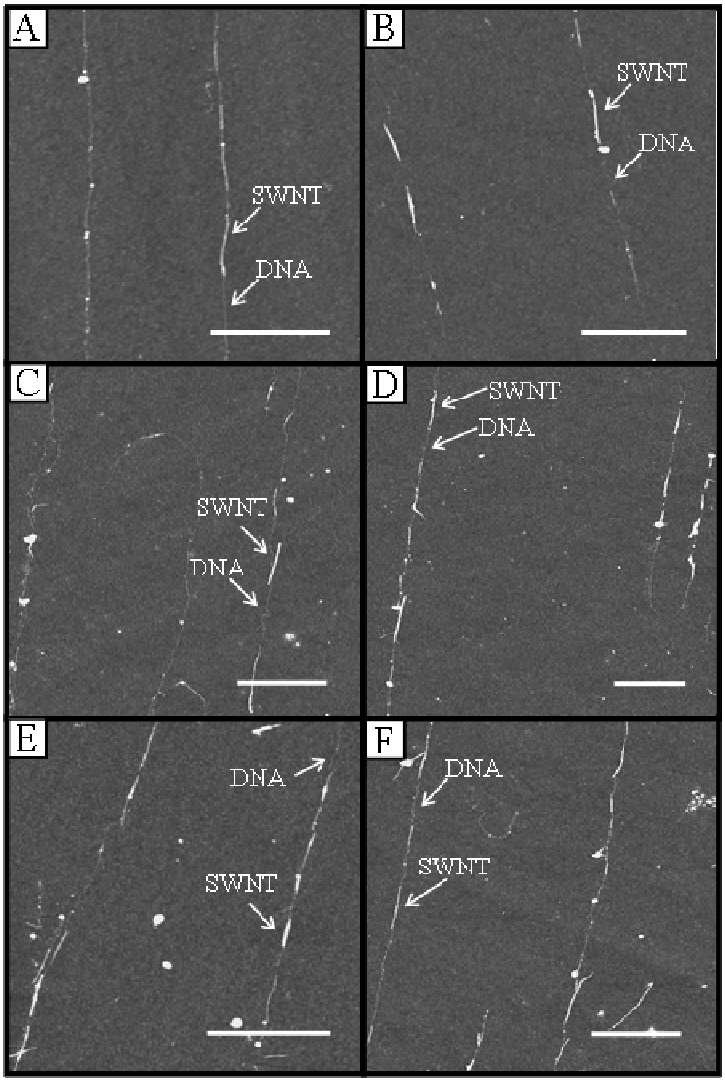

Figure 4.3 AFM height images of DNA-templated SWNT positioning using a fourfold diluted DTAB-wrapped SWNT suspension. (A-C) Three different DNA surfaces after one SWNT suspension treatment. (D-F) Three different DNA surfaces following three DTAB-wrapped SWNT treatments. The height scale is 5 nm, and the white bars are 1 μm in all images.

greater than those of the DNA. Deposition of the fourfold diluted SWNT suspension on surfaces like the one in Figure 4.2A resulted in a DNA coverage of 18%, with a localization selectivity of 80%; representative AFM images of these substrates are shown in Figure 4.3A-C. I attribute the high degree of selectivity of SWNTs for DNA (compared to the rest of the surface) to the positive charges from immobilized poly-L-lysine, which should repel the positively charged DTAB head groups on wrapped

SWNTs. The DNA coverage increased to 33% and 46% after two and three treatments with the same SWNT suspension, respectively, while the localization selectivities remained essentially constant at 80% and 79%, respectively. Figure 4.3D-F shows representative AFM images from three surfaces after three treatments with the diluted SWNT suspension. DNA coverage did not increase beyond 49%, even after six total treatments with the diluted SWNT suspension. This plateauing of SWNT coverage of DNA may be caused by the deposition of free DTAB molecules on the surface DNA, hindering the interaction between DTAB-wrapped SWNTs and DNA.

4.3.3 SWNT Deposition from Concentrated Solutions

With an undiluted, freshly prepared SWNT suspension, a single deposition led to an average DNA coverage of 83%, with a localization selectivity of 76%. Nearly continuous nanotube assemblies were formed, as shown in Figure 4.4A-C, where SWNTs and SWNT bundles cover most of the DNA, with only a few small (<200 nm) gaps between SWNTs. Figure 4.4D-E contains larger-area AFM images, which demonstrate that the SWNT deposition is uniform over length scales nearing ten microns. Additional treatments of these surfaces with fresh SWNT suspension did not increase coverage further. This may be due to the already deposited DTAB-wrapped SWNTs on DNA electrostatically repelling additional DTAB-wrapped SWNTs in suspension, or because the gaps between localized SWNTs were smaller than the typical lengths (200-600 nm) of SWNTs in suspension. Importantly, with these improved experimental techniques, aligned surface DNA molecules are mostly covered with SWNTs.

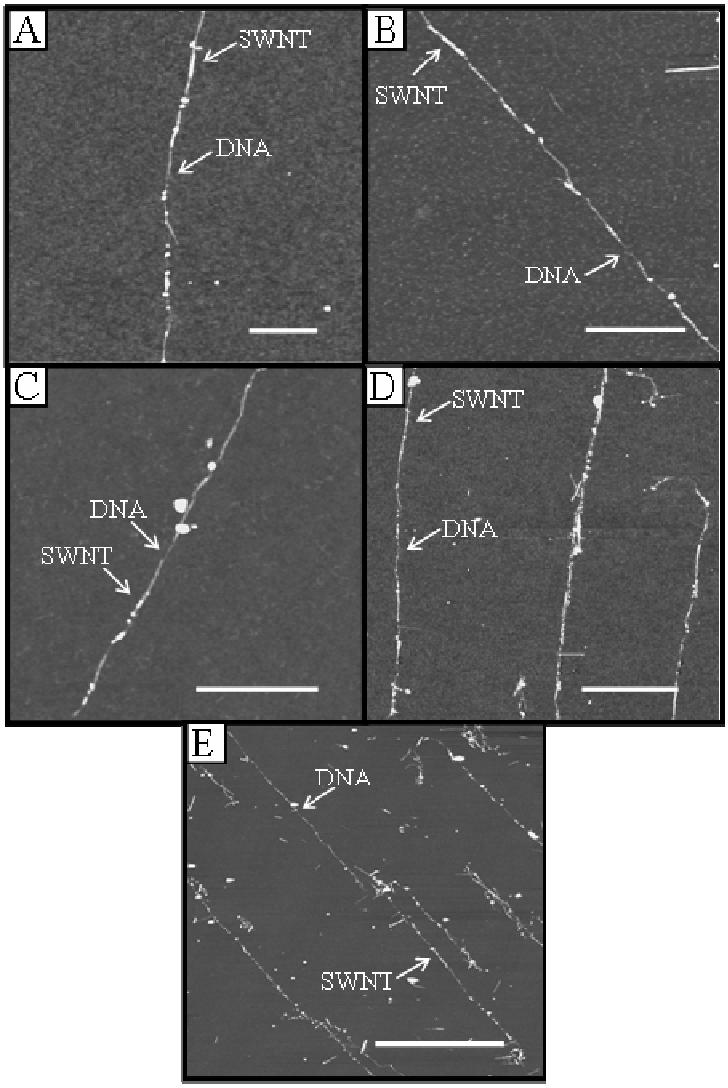

Figure 4.4 AFM height images of DTAB-wrapped SWNT placement on DNA. (A-C) Three DNA surfaces after one treatment with freshly prepared DTAB-wrapped SWNTs. (D-E) Larger-area images of the surfaces shown in (A-B). The height scale is 5 nm in all images. The white bars represent 500 nm in (A-C), 1 μm in (D) and 3 μm in (E).

4.4 Conclusions

I have developed a straightforward approach for constructing aligned surface SWNT assemblies. In this method, SWNTs are manipulated in aqueous media without the need for complicated chemical functionalization, and the positioning of SWNTs is

controlled through the surface arrangement of DNA. With low-concentration SWNT suspensions, multiple treatments (up to three) provide DNA coverage of nearly 50%, and with higher-concentration freshly made SWNT suspensions, largely continuous linear SWNT assemblies are formed with a single treatment. I plan to investigate the electronic properties of these DNA-templated SWNT assemblies (see Chapter 5) and explore methods for filling any gaps with metal to enhance the conductivity of these constructs. This work shows important progress toward making continuously connected aligned SWNTs assemblies, which could serve as nanowires in nanoelectronic circuits.

4.5 References

1. Madou, M. J. *Fundamentals of Microfabrication: The Science of Miniaturization* 2nd edn, Boca Raton, FL, CRC Press, **2002**.
2. Timp, G. L. (ed) *Nanotechnology*, New York, Springer, **1999**.
3. Braun, E.; Eichen, Y.; Sivan, U.; Ben-Yoseph, G. DNA-Templated Assembly and Electrode Attachment of a Conducting Silver Wire, *Nature* **1998**, *391*, 775-778.
4. Becerril, H. A.; Stoltenberg, R. M, Monson, C. F; Woolley, A. T. Ionic Surface Masking for Low Background in Single- and Double-Stranded DNA-Templated Silver and Copper Nanorods, *J. Mater. Chem.* **2004**, *14*, 611-616.
5. Richter. J.; Mertig, M.; Pompe. W.; Mönch, I.; Schackert, H. K. Construction of Highly Conductive Nanowires on a DNA Template, *Appl. Phys. Lett.* **2001**, *78*, 536-538.
6. Ford, W. E.; Harnack, O.; Yasuda, A.; Wessels, J. M. Platinated DNA as Precursors to Templated Chains of Metal Nanoparticles, *Adv. Mater.* **2001**, *13*, 1793-1797.
7. Ongaro, A.; Griffin, F.; Beecher, P.; Nagle, L.; Iacopino, D.; Quinn, A.; Redmond, G.; Fitzmaurice, D. DNA-Templated Assembly of Conducting Gold Nanowires between Gold Electrodes on a Silicon Oxide Substrate, *Chem. Mater.* **2005**, *17*, 1959-1964.
8. Keren, K.; Berman, R. S.; Buchstab, E.; Sivan, U.; Braun, E. DNA-Templated Carbon Nanotube Field-Effect Transistor, *Science* **2003**, *302*, 1380-1382.
9. Monson, C. F.; Woolley, A. T. DNA-Templated Construction of Copper Nanowires, *Nano Lett.* **2003**, *3*, 359-363.
10. Xin, H.; Woolley, A. T. DNA-Templated Nanotube Localization, *J. Am. Chem. Soc.*

2003, *125*, 8710-8711.

11. Kong, J.; Franklin, N. R.; Zhou, C.; Chapline, M, G.; Peng, S.; Cho, K.; Dai, H. Nanotube Molecular Wires as Chemical Sensors, *Science* **2000**, *287*, 622-625.
12. Snow, E. S.; Perkins, F. K.; Houser, E. J.; Badescu, S. C.; Reinecke, T. L. Chemical Detection with a Single-Walled Carbon Nanotube Capacitor, *Science* **2005**, *307*, 1942-1945.
13. Zhou, Y.; Gaur, A.; Hur, S-H.; Kocabas, C.; Meitl, M. A.; Shim, M.; Rogers, J. A. p-Channel, n-Channel Thin Film Transistors and p-n Diodes Based on Single Wall Carbon Nanotube Networks, *Nano Lett.* **2004**, *4*, 2031-2035.
14. Collins, P. G.; Zettl, A.; Bando, H.; Thess, A.; Smalley, R. E. Nanotube Nanodevice, *Science* **1997**, *278*, 100-103.
15. Derycke, V.; Martel, R.; Appenzeller, J.; Avouris, Ph. Carbon Nanotube Inter- and Intramolecular Logic Gates, *Nano Lett.* **2001**, *1*, 453-456.
16. Bahr, J. L.; Mickelson, E. T.; Bronikowski, M. J.; Smalley, R. E.; Tour, J. M. Dissolution of Small Diameter Single-Wall Carbon Nanotubes in Organic Solvents? *Chem. Commun.* **2001**, 193-194.
17. Chen, J. Rao, A.M.; Lyuksyutov, S.; Itkis, M. E.; Hamon, M. A.; Hu, H.; Cohn, R. W.; Eklund, P. C.; Colbert, D. T.; Smalley, R. E.; Haddon, R. C. Dissolution of Full-Length Single-Walled Carbon Nanotubes *J. Phys. Chem. B* **2001**, *105*, 2525-2528.
18. Pompeo, F.; Resasco, D. E. Water Solubilization of Single-Walled Carbon Nanotubes by Functionalization with Glucosamine, *Nano Lett.* **2002**, *2*, 369-373.
19. O'Connell, M. J.; Boul, P.; Ericson, L. M.; Huffman, C.; Wang, Y.; Haroz, E.; Kuper, C.; Tour, J.; Ausman, K. D.; Smalley, R. E. Reversible Water-Solubilization of

Single-Walled Carbon Nanotubes by Polymer Wrapping, *Chem. Phys. Lett.* **2001**, *342*, 265-271.

20. Zheng, M.; Jagota, A.; Semke, E. D.; Diner, B. A.; Mclean, R. S.; Lustig, S. R.; Richardson, R. E.; Tassi, N. G. DNA-Assisted Dispersion and Separation of Carbon Nanotubes, *Nat. Mater.* **2003**, *2*, 338-342.
21. Liu, J.; Rinzler, A. G.; Dai, H.; Hafner, J. H.; Bradley, R. K.; Boul, P. J.; Lu, A.; Iverson, T.; Shelimov, K.; Huffman, C. B.; Rodriguez-Macias, F.; Shon, Y.-S.; Lee, T. R.; Colbert, D. T.; Smalley, R. E. Fullerene Pipes, *Science* **1998**, *280*, 1253-1256.
22. Moore, V. C.; Strano, M. S.; Haroz, E. H.; Hauge, R. H.; Smalley, R. E.; Schmidt, J.; Talmon, Y. Individually Suspended Single-Walled Carbon Nanotubes in Various Surfactants, *Nano Lett.* **2003**, *3*, 1379-1382.
23. O'Connell, M. J.; Bachilo, S. M.; Huffman, C. B.; Moore, V. C.; Strano, M. S.; Haroz, E. H.; Rialon, K. L.; Boul, P. J.; Noon, W. H.; Ma, J.; Hauge, R. H.; Weisman, R. B.; Smalley, R. E. Band Gap Fluorescence from Individual Single-Walled Carbon Nanotubes, *Science* **2002**, *297*, 593-596.
24. Matarredona, O.; Rhoads, H.; Li, Z.; Harwell, J. H.; Balzano, L.; Resasco, D. E. Dispersion of Single-Walled Carbon Nanotubes in Aqueous Solutions of the Anionic Surfactant NaDDBS, *J. Phys. Chem. B* **2003**, *107*, 13357-13367.
25. Islam, M. F.; Rojas, E.; Bergey, D. M.; Johnson, A. T.; Yodh, A. G. High Weight Fraction Surfactant Solubilization of Single-Wall Carbon Nanotubes in Water, *Nano Lett.* **2003**, *3*, 269-273.
26. Strano, M. S.; Moore, V. C.; Miller, M. K.; Allen, M. J.; Haroz, E. H.; Kittrell, C.; Hauge, R. H.; Smalley, R. E. The Role of Surfactant Adsorption During

Ultrasonication in the Dispersion of Single-Walled Carbon Nanotubes, *J. Nanosci. Nanotechnol.* **2003**, *3*, 81-86.

27. Baker, S. E.; Cai, W.; Lasseter, T. L.; Weidkamp, K. P.; Hamers, R. J. Covalently Bonded Adducts of Deoxyribonucleic Acid (DNA) Oligonucleotides with Single-Wall Carbon Nanotubes: Synthesis and Hybridization, *Nano Lett.* **2002**, *2*, 1413-1417.
28. Dwyer, C.; Guthold, M.; Falvo. M.; Washburn, S.; Superfine, R.; Erie, D. DNA-Functionalized Single-Walled Carbon Nanotubes, *Nanotechnology* **2002**, *13*, 601-604.
29. Lustig, S. R.; Jagota, A.; Khripin, C.; Zheng, M. Theory of Structure-Based Carbon Nanotube Separations by Ion-Exchange Chromatography of DNA/CNT Hybrids, *J. Phys. Chem.* B **2005**, *109*, 2559-2566.
30. Li, S.; He, P.; Dong, J.; Guo, Z.; Dai, L. DNA-Directed Self-Assembling of Carbon Nanotubes, *J. Am. Chem. Soc.* **2005**, *127*, 14-15.
31. Dresselhaus, M. S.; Dresselhaus, G.; Avouris, Ph. (ed) *Carbon Nanotubes: Synthesis, Structure, Properties, and Applications*, Berlin, Springer, **2001**.
32. Woolley, A. T.; Kelly, R. T. Deposition and Characterization of Extended Single-Stranded DNA Molecules on Surfaces, *Nano Lett.* **2001**, *1*, 345-348.

CHAPTER 5: ELECTRONIC PROPERTIES OF DNA-TEMPLATED SINGLE-WALLED CARBON NANOTUBES

5.1 Introduction

The investigation and application of the electrical properties of carbon nanotubes (CNTs) have attracted extensive attention. Various electronic characteristics of different types of CNTs have been explored. Dekker et al. studied the electrical transport properties of individual metallic single-walled carbon nanotubes (SWNTs) [1]. From current versus voltage (I-V) measurements, they found that current increased almost linearly with voltage, indicative of quantum wire behavior for metallic SWNTs. Lieber et al. demonstrated a correlation between structural defects and conductivity in multi-walled carbon nanotubes (MWNTs) [2]. Their results showed that conductivities of perfect, defect-free nanotubes were an order of magnitude higher than in CNTs with defects. Haddon et al. measured the conductivity of films of as-prepared and purified SWNTs to be 250-400 S/cm [3]. In contrast, the conductivities of octadecylamine- and poly(*m*-aminobenzenesulfonic acid)-functionalized SWNT films were 2-3 orders of magnitude lower. McEuen et al. measured electrical transport in ropes of SWNTs [4]. They found that the conductance was suppressed near zero voltage at temperatures lower than 10 K,

and the gate voltage modulated the number of conduction electrons in the SWNT ropes. These effects were indicative of single-electron charging and resonant tunneling through the quantized energy levels of ropes of SWNTs.

Because of their unique electronic properties, CNTs have been used to fabricate field-effect transistors (FETs) [5-7] and chemical sensors [8]. Avouris et al. constructed FETs using SWNTs and MWNTs [6]. In the SWNT-FET devices, the conductance could be modulated over five orders of magnitude with the gate voltage. The MWNT-FETs showed no gate effects, but structurally deformed MWNTs had FET behavior. Li et al. fabricated a SWNT sensor platform [8], which could sense NO_2 gas and organic vapors (acetone, benzene and nitrotoluene) by detecting changes in SWNT conductance.

The electronic properties of CNTs can be probed using scanning tunneling microscopy [9] or conductive atomic force microscopy (AFM) [10, 11] by scanning a tip along the length of CNTs. The connection of CNTs with microelectrodes is not critical in these scanning probe microscopy measurement methods. Two techniques, which require contacts of CNTs to electrodes, are used more widely for the study of electrical properties of CNTs and their application in devices. The first approach involves depositing a CNT suspension [12] or growing CNTs by chemical vapor deposition (CVD) [5] on substrates, and then fabricating contacts using lithography techniques. This method generates high-quality contacts between CNTs and the electrodes, but requires sophisticated techniques (e.g., electron beam lithography) to pattern the contacts. The second approach proceeds in the opposite order: a dispersed SWNT suspension is deposited [13] or SWNTs are grown [14] on substrates on which contacts have already been fabricated. In this strategy, the electrodes are easier to make, but the positions of the CNTs are more difficult to control,

and contact quality varies significantly.

Previously, I have localized SWNTs on DNA templates on Si using two approaches. The first, described in Chapter 3, utilized a bifunctional compound (1-pyrenemethylamine) bridging between DNA and SWNTs [15]. In Chapter 4, a cationic surfactant, dodecyltrimethylammonium bromide (DTAB), was used to disperse SWNTs in aqueous solution and localize them on DNA templates through electrostatic interactions [16]. In this chapter, I used the same methods as in Chapter 4 to localize DTAB-wrapped SWNTs on DNAs, which were prealigned across microelectrodes, and the I-V properties of individual DNA-templated SWNTs were measured. In this technique, the placement of SWNTs depends on the positions of the prealigned DNAs. Importantly, this procedure provides a simple way to localize SWNTs across electrodes in a controlled manner, which may be useful in the fabrication of nanoelectronic devices using SWNTs.

5.2 Experimental Section

The gold microelectrodes were fabricated using standard UV lithography techniques. An electrode layout was made using computer-aided design software and then patterned on a glass-chromium photolithographic mask using monochromatic UV light in an Electromask (TRE, Santa Ana, CA) pattern generator. Next, a 500-nm-thick thermal oxide layer was grown on p-type silicon <100> wafers (TTI Silicon, Sunnyvale, CA) using a tube furnace (Bruce Technologies, Billerica, MA). The wafers were coated with a 300-nm-thick layer of AZ-3312 positive photoresist (AZ Electronic Materials, Somerville, NJ) using a spinner (Laurell, North Wales, PA) and soft baked for 60 s at 90 °C prior to

exposure. The photoresist-coated wafers were exposed to monochromatic UV light using the step-and-repeat mode of the pattern generator for improved resolution of small features in the electrode pattern. Exposed wafers were soft baked at 110 °C for 60 s and immersed for 60 s in AZ-300 developer solution (AZ Electronic Materials). Exposed silicon dioxide regions on the wafers were cleaned with a ~10-s dip in buffered oxide etch (Baker, Phillipsburg, NJ), and the substrates were placed in a CHA-600 triple-source thermal evaporator (CHA, Fremont, CA). Approximately 5 nm of Cr and 35 nm of Au were deposited on the wafers, and the excess metal and photoresist were removed from the patterns by an acetone lift-off step, followed by a 30-s dip in freshly prepared piranha solution (a 7:3 mixture of concentrated sulfuric acid and 30% hydrogen peroxide).

SWNT (Carbon Nanotechnologies, Houston, TX) suspensions were prepared in 1% aqueous DTAB solution following a previously developed method outlined in Section 4.2.1 [16]. An electrode-patterned substrate was incubated with 40 μL of 10 μg/mL aqueous poly-L-lysine solution for 5 min. A 1 μL droplet of double-stranded λ DNA solution (10 μg/mL) was translated across the electrodes to align DNA [17]. The surface was then treated with fresh SWNT suspension for 10 min. Between each step, the substrate was rinsed thoroughly with deionized water and dried under a stream of nitrogen.

All substrates were studied by AFM. Images were taken with a Multimode IIIa AFM setup (Veeco, Sunnyvale, CA) using aluminum-coated silicon tips (Budgetsensors, Sofia, Bulgaria). Vibrational noise was damped with an active isolation system (MOD1-M, Halcyonics, Goettingen, Germany). AFM imaging parameters were as follows: tip resonance frequency, ~300 kHz; free oscillation amplitude, 0.9-1.1 V; set-point, 0.3-0.9

V; scan rate, 0.4-1.6 Hz. All images were processed after acquisition to eliminate background curvature.

The I-V curves were measured at room temperature under ambient conditions using a system combining an E5262 two-channel high-speed source monitor unit (Agilent, Palo Alto, CA) with a low-noise probe station (Micromanipulator Inc., Carson City, NV). The scan range was from -0.1 to +0.1 V for SWNT samples and from -0.5 to +0.5 V for control surfaces. Tungsten probe tips, with a point radius of 0.5 µm, contacted the microelectrodes.

5.3 Results and Discussion

Figure 5.1 shows a photograph of the gold microelectrodes that DNA (and SWNTs) were aligned across for I-V measurements. The electrodes were designed with gaps ranging from small (<500 nm) to large (~500 µm). From 35 substrates measured, the smallest distance between the A/B electrodes and the C electrode was between 200 and 1,000 nm, with a considerable fraction (~50%) between 450-550 nm, which was in the range of typical suspended SWNT lengths [16]. This setup was designed such that individual SWNTs could be localized bridging the electrodes on prealigned surface DNA in the small-gap area.

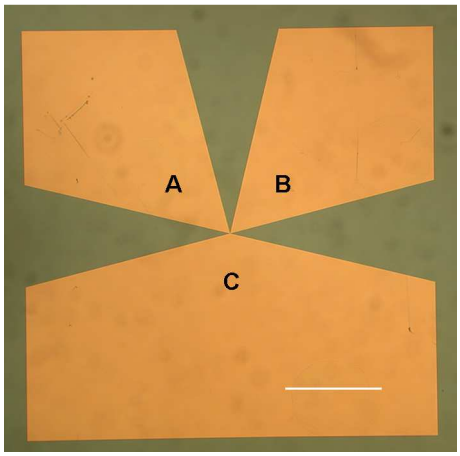

Figure 5.1 Photograph of the microelectrode design. A, B, and C are lithographically patterned gold microelectrodes. The scale bar represents 500 µm.

DNA molecules were deposited directionally across the space between the A/B and C electrodes. In the various batches of substrates, the electrodes were elevated from 5-20 nm above the Si surface. If the electrode surfaces were >10 nm higher than the Si, DNA deposition was very sparse. In this study, the electrodes were ~6 nm taller than the Si surface, which provided adequate coverage of DNA on the substrate. Figure 5.2A and Figure 5.2D show AFM data of DNA aligned on the surface across electrodes.

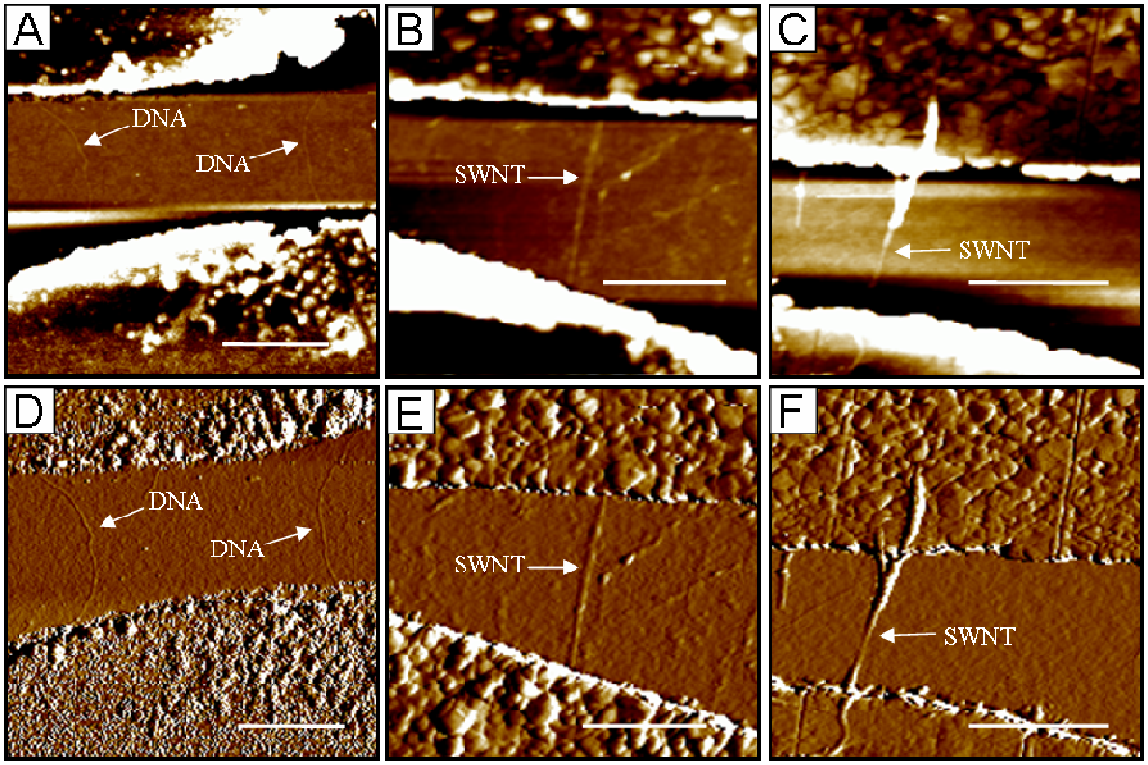

Figure 5.2 AFM height (A-C) and amplitude (D-F) images of DNA and DNA-templated SWNTs deposited on electrodes. (A, D) DNA aligned across electrodes prior to SWNT localization. (B, E) A DNA-templated SWNT between electrodes. (C, F) A DNA-templated SWNT on top of and bridging electrodes. The scale bars represent 500 nm in all images. The DNA and SWNTs are labeled by arrows.

AFM images in Figure 5.2B-C and Figure 5.2E-F present individual SWNTs localized on prealigned DNA traversing electrodes. On most substrates, SWNT deposition was similar to that shown in Figure 5.2B and Figure 5.2E, where a SWNT was on the surface between electrodes, but did not have obvious contact with the tops of the

electrodes. In an atypical SWNT placement, shown in Figure 5.2C and Figure 5.2F, a SWNT was deposited on top of both electrodes and bridging the gap.

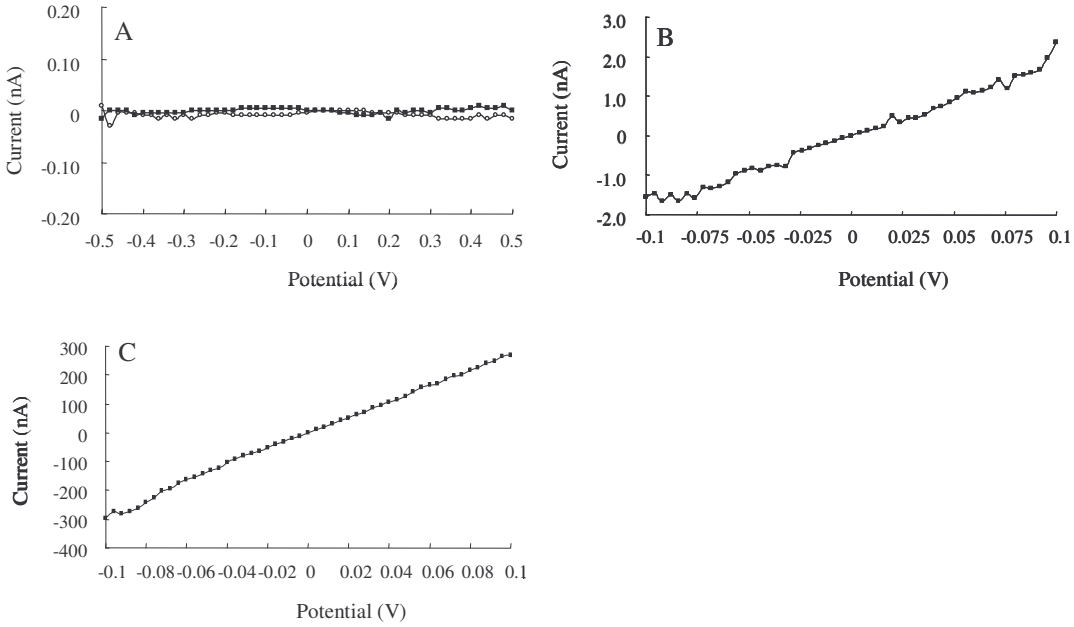

Figure 5.3 I-V curves from control substrates and DNA-templated SWNTs across electrodes. (A) Control substrates: (—○—) an untreated electrode surface; (—■—) a substrate with aligned DNA that was treated with 1% DTAB lacking SWNTs. (B) A substrate with a SWNT between electrodes (Figure 5.2B). (C) A substrate with a SWNT on top of and bridging electrodes (Figure 5.2C).

I-V properties of various surfaces are reported in Figure 5.3. The I-V curves in Figure 5.3A were from two control surfaces: an electrode substrate prior to any treatments and a substrate with DNA aligned across electrodes and which was treated with 1% DTAB lacking SWNTs. The conductance of these control surfaces was $<10^{-12}$ S. The I-V curves in Figure 5.3B-C were from the SWNTs in Figure 5.2B-C. The conductance of the SWNT in Figure 5.2B was 1.7×10^{-8} S. The SWNT with contacts to the tops of the electrodes in Figure 5.2C had a conductance of 2.2×10^{-6} S, which was

~130 times higher than the one in Figure 5.2B. Substrates with SWNT placement similar to that in Figure 5.2B had conductance values in the range of 7.3×10^{-9}-4.8×10^{-8} S (see Table 5.1). It appears that the contact resistance is considerably lower when SWNTs are located on top of the electrodes, compared to when SWNTs are placed between electrodes.

Table 5.1. Conductance of DNA-Templated SWNTs on Five Substrates

Substrate	Length (nm)	Resistance (Ω)	Conductance (S)
1	730	1.4×10^{8}	7.3×10^{-9}
2	500	1.0×10^{8}	1.0×10^{-8}
3	560	5.9×10^{7}	1.7×10^{-8}
4	680	2.1×10^{7}	4.8×10^{-8}
5*	410	4.5×10^{5}	2.2×10^{-6}

* Substrate shown in Figure 5.2C.

With perfect contacts and two electron transport channels, the conductance of a metallic SWNT should be $4e^2/h$ = 155 μS (e is the electron charge and h is Planck's constant), which corresponds to a resistance of 6.45 kΩ [18]. Imperfect connections to the electrodes add a contact resistance (R_c) to the total resistance [19]. Individual SWNT resistances of ~1 MΩ [20] and 2.9 MΩ [6] at room temperature have been reported. With improved contacts made using titanium, Dai et al. reported a resistance of 11 kΩ for an individual SWNT at room temperature [18]. In my work, when a SWNT was on top of the electrodes, the resistance was 450 kΩ, which is slightly less than the values reported by Tans [20] and Avouris [6], but much higher than the literature value for a SWNT with almost perfect electrical contacts [18]. The other substrates, where SWNTs bridged

electrodes, but lacked obvious contacts to the tops of the electrodes, had 100-500 fold higher resistances, which indicates the possibility of small gaps between the SWNT ends and the electrodes.

5.4 Conclusions and Future Work

This work demonstrates that DNA-templated SWNTs can be formed across electrodes on surfaces, providing a new approach for localizing SWNTs across contacts in a controlled manner. When a DNA-templated SWNT was placed on top of and bridging electrodes, the measured conductance was comparable to literature values. On the other hand, SWNTs that lacked contacts to the tops of electrodes had conductance values hundreds of times lower than those in the literature, probably due to gaps between SWNTs and electrodes. My approach for controlled surface placement of SWNTs may be useful in making nanoelectronic or nanomechanical devices.

In the future, it will be critical to optimize the connections between SWNTs and electrodes. One potential improvement would be to have the electrodes level with the Si surface, so there is no height difference between the electrodes and Si. In this way, the DNAs should deposit on top of the electrodes more readily, and SWNTs should thus be localized on top of electrodes, as in Figure 5.2C. An alternative method to solve the contact problem would be to deposit metal, such as Au or Cu, into the gaps between SWNTs and electrodes to decrease the contact resistance. These improvements should move the measured electrical properties of SWNTs closer to theoretical values.

5.5 References

1. Venema, L. C.; Wildöer, J. W. C.; Janssen, J. W.; Tans, S. J.; Tuinstra, H. L. J.; Kouwenhoven, L. P.; Dekker, C. Imaging Electron Wave Functions of Quantized Energy Levels in Carbon Nanotubes, *Science* **1999**, *283*, 52-55.
2. Dai, H.; Wong, E. W.; Lieber, C. M. Probing Electrical Transport in Nanomaterials: Conductivity of Individual Carbon Nanotubes, *Science* **1996**, *272*, 523-526.
3. Bekyarova, E.; Itkis, M. E.; Cabrera, N.; Zhao, B.; Yu, A.; Gao, J.; Haddon, R. C. Electronic Properties of Single-Walled Carbon Nanotube Networks, *J. Am. Chem. Soc.* **2005**, *127*, 5990-5995.
4. Bockrath, M.; Cobden, D. H.; McEuen, P. L.; Chopra, N. G.; Zettl, A.; Thess, A.; Smalley, R. E. Single-Electron Transport in Ropes of Carbon Nanotubes, *Science* **1997**, *275*, 1922-1925.
5. Bradley, K.; Cumings, J.; Star, A.; Gabriel, J.-C. P.; Grüner, G. Influence of Mobile Ions on Nanotube Based FET Devices, *Nano Lett.* **2003**, *3*, 639-641.
6. Martel, R.; Schmidt, T.; Shea, H. R.; Hertel, T.; Avouris, Ph. Single- and Multi-Wall Carbon Nanotube Field-Effect Transistors, *Appl. Phys. Lett.* **1998**, *73*, 2447-2449.
7. Auvray, S.; Derycke, V.; Goffman, M.; Filoramo, A.; Jost, O.; Bourgoin, J.-P. Chemical Optimization of Self-Assembled Carbon Nanotube Transistors, *Nano Lett.* **2005**, *5*, 451-455.
8. Li, J.; Lu, Y.; Ye, Q.; Cinke, M.; Han, J.; Meyyappan, M. Carbon Nanotube Sensors for Gas and Organic Vapor Detection, *Nano Lett.* **2003**, *3*, 929-933.
9. Collins, P. G.; Zettl, A.; Bando, H.; Thess, A.; Smalley, R. E. Nanotube Nanodevice, *Science* **1997**, *278*, 100-103.

10. Bockrath, M.; Markovic, N.; Shepard, A.; Tinkham, M.; Gurevich, L.; Kouwehoven, L. P.; Wu, M. W.; Sohn, L. L. Scanned Conductance Microscopy of Carbon Nanotubes and λ-DNA, *Nano Lett.* **2002**, *2*, 187-190.

11. Heo, J.; Bockrath, M. Local Electronic Structure of Single-Walled Carbon Nanotubes from Electrostatic Force Microscopy, *Nano Lett.* **2005**, *5*, 853-857.

12. Misewich, J. A.; Martel. R.; Avouris, Ph.; Tsang, J. C.; Heinze, S.; Tersoff, J. Electrically Induced Optical Emission from a Carbon Nanotube FET, *Science* **2003**, *300*, 783-786.

13. Derycke, V.; Martel, R.; Appenzeller, J.; Avouris, Ph. Carbon Nanotube Inter- and Intramolecular Logic Gates, *Nano Lett.* **2001**, *1*, 453-456.

14. Biercuk, M. J.; Mason, N.; Marcus, C. M. Local Gating of Carbon Nanotubes, *Nano Lett.* **2004**, *4*, 1-4.

15. Xin, H.; Woolley, A. T. DNA-Templated Nanotube Localization, *J. Am. Chem. Soc.* **2003**, *125*, 8710-8711.

16. Xin, H.; Woolley, A. T. High-Yield DNA-Templated Assembly of Surfactant-Wrapped Carbon Nanotubes, *Nanotechnology* **2005**, *16*, 2238-2241.

17. Woolley, A. T.; Kelly, R. T. Deposition and Characterization of Extended Single-Stranded DNA Molecules on Surfaces, *Nano Lett.* **2001**, *1*, 345-348.

18. Kong, J.; Yenilmez, E.; Tombler, T. W.; Kim, W.; Dai, H. Quantum Interference and Ballistic Transmission in Nanotube Electron Waveguides, *Phys. Rev. Lett.* **2001**, *87*, 106801-106804.

19. McEuen, P. L.; Fuhrer, M.; Park, H. Single-Walled Carbon Nanotube Electronics, *IEEE Trans. Nanotechnol.* **2002**, *1*, 78-85.

20. Tans, S. J.; Devoret, M. H.; Dai, H.; Thess, A.; Smalley, R. E.; Geerligs, L. J.; Dekker, C. Individual Single-Wall Carbon Nanotubes as Quantum Wires, *Nature* **1997**, *386*, 474-477.

CHAPTER 6: CONCLUSIONS AND FUTURE WORK

6.1 Conclusions

6.1.1 Alignment of SWNTs on Surfaces

In Chapter 2, I described a method that enables facile control of the orientation of single-walled carbon nanotubes (SWNTs) over the entire area of several-millimeter-scale Si surfaces. When Ar flow was applied over a SWNT suspension droplet, nanotubes were aligned on the surface with the same orientation as the Ar flow direction. The gas flow linear velocity was critical in this approach. Ar flow rates of 6-9 cm/s led to nicely aligned SWNTs; under other flow conditions, the nanotubes were oriented randomly. Two-dimensional orthogonal SWNT arrangements were also achieved using a two-step process with this approach. Based on time-lapse imaging of the movements of SWNT aggregates under Ar flow, I hypothesize that the circulation of SWNTs in suspension within a droplet, combined with the attraction between the amine groups in poly-L-lysine and the SWNT sidewalls, leads to the deposition of aligned SWNTs on the surface.

Compared with directed growth methods to control the orientation of SWNTs [1, 2], my post-growth SWNT manipulation technique is very simple. This approach could potentially be used to control SWNT orientation on surfaces in the fabrication of nanodevices.

6.1.2 DNA-Templated SWNT Localization

I developed two new methods for SWNT localization on DNA templates, which are presented in Chapters 3 and 4.

In Chapter 3, I showed that SWNTs could be anchored on 1-pyrenemethylamine (PMA)-coated DNA. In this approach, over 60% of all SWNTs deposited on substrates were aligned on DNA fragments, which indicated the feasibility of using DNA as a template for localizing SWNTs. The PMA played a key role in SWNT placement; indeed, without PMA bridging between the SWNTs and DNA, nanotubes were not selectively deposited on surface DNA molecules. By arranging the placement of surface DNAs, the positions of SWNTs could also be controlled to some degree. Coverage of DNA with SWNTs was only ~5%, but it was hypothesized that increasing the concentration of SWNTs would improve the DNA coverage. This technique offers a novel approach to facilitate SWNT deposition onto surface DNA, and it could be useful in the bottom-up construction of nanoscale electronic devices with SWNTs.

In Chapter 4, SWNTs were localized on DNA templates with the assistance of a cationic surfactant, dodecyltrimethylammonium bromide (DTAB). SWNT positioning was controlled by the surface DNA arrangement, and the extent of deposition was influenced by the SWNT concentration. With lower-concentration SWNT suspensions, multiple surface treatments increased the DNA coverage. Using freshly prepared, undiluted SWNT suspension, 83% of the length of surface DNAs was covered with SWNTs, and 76% of all surface-deposited SWNTs were on the DNA. In some regions, nearly continuous SWNT assemblies were formed. Further optimization of the sonication time and DTAB concentration may make it possible to increase the concentration of

SWNTs in the DTAB solution, which should increase DNA coverage even more. DNA-templated deposition of surfactant-wrapped nanotubes may be useful in SWNT nanowire fabrication for nanoelectronics.

The method for surfactant-wrapped SWNT localization on DNA, outlined in Chapter 4, has important advantages over the PMA bridging approach described in Chapter 3. First, DTAB is less toxic than PMA, which is preferable for researchers and the environment. Second, SWNTs dispersed in aqueous solution, rather than organic solvents, are more compatible with potential applications in the bottom-up fabrication of nanodevices. Finally, the DNA coverage of SWNTs increased from 5% to 83%, a greater than 15-fold improvement, by using DTAB-wrapped SWNTs.

6.1.3 Electrical Measurements on DNA-Templated SWNT Assemblies

In Chapter 5, DNA-templated SWNTs were placed across electrodes, and the electronic properties of these constructs were measured. From current vs. voltage measurements, the resistance and conductance of these DNA-templated SWNTs were obtained. When a DNA-templated SWNT was placed on top of and bridging electrodes, its measured conductance was close to literature values. In contrast, when a SWNT was between electrodes without contacting their tops, its measured conductance was hundreds of times lower than literature values, which revealed the potential presence of small gaps between the SWNT and electrodes. In Chapter 5, I showed that DTAB-wrapped SWNTs can be localized on DNA on electrode surfaces, and the electronic property measurements of these SWNTs revealed that this technique has potential for application in the fabrication of nanodevices with SWNTs.

6.2 Future Work

6.2.1 Fabrication of Continuous SWNT Nanowires

In Chapter 4, I demonstrated that nearly continuous SWNT assemblies could be deposited on DNA fragments, but there were small gaps between SWNTs. For SWNTs to serve as nanowires in nanodevices, these insulating gaps must be filled with conducting material. One potential solution to this issue is to use metal, such as Ag (Figure 6.1), to fill the gaps. DNA-templated Ag nanowires have been reported previously [3, 4], and have been shown to be electrically conductive [3]. Thus, after a DNA has been coated with SWNTs, the exposed DNA segments could be metallized with Ag to fill the gaps and create a conductive construct that could serve as a nanowire. This approach would result in junctions between SWNTs and Ag, so the effects of these interfaces on the electrical conductivity of the nanowires would need to be explored.

Figure 6.1 A DNA-templated SWNT/Ag nanowire.

6.2.2 Fabrication of SWNT Transistors

DNA-templated SWNT field-effect transistors (FETs) have been fabricated previously [5]. In these devices, the DNA fragments were metallized with Ag and Au, which acted as contacts. Using the approach for SWNT localization I presented in Chapter 4, it should be feasible to fabricate FETs of a similar design. After a single semiconducting SWNT is localized on a DNA template with an appropriate SWNT concentration, the uncovered DNA segments on both sides of the SWNT could be metallized with Ag, followed by Au (Figure 6.2). This strategy might not require the

fabrication of contact electrodes using traditional (and more costly) lithography methods. The effectiveness of this proposed DNA-templated SWNT-FET fabrication scheme should be investigated.

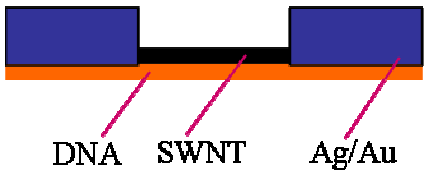

Figure 6.2 A DNA-templated SWNT transistor.

6.2.3 Fabrication of SWNT Chemical Sensors

Based on the work presented in Chapter 5, chemical sensors that detect changes in SWNT conductance/resistance when the devices are exposed to gases could be fabricated [6, 7]. However, the contact resistance at the electrodes would need to be reduced first, which I propose to do in several ways. First, by optimizing the fabrication, the electrodes could be made at the same level as the Si surface, so DNA could be aligned more easily on top of and bridging electrodes (Figure 6.3). Second, the gaps between SWNTs and electrodes could be filled with metal such as Ag, as described in Section 6.2.1. Application of these two methods should solve the gap problem between SWNTs and electrodes. In addition, good contacts between metal and SWNTs can be achieved using titanium electrodes [8]. Thus, the use of titanium instead of gold to construct electrodes should further reduce the contact resistance.

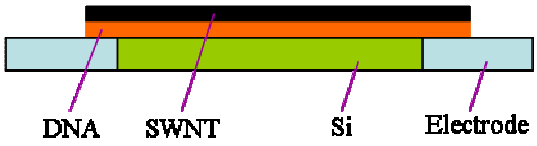

Figure 6.3 A DNA-templated SWNT placed on top of and bridging electrodes.

SWNTs have been used as chemical sensors to detect gases. Dai et al. reported that when a semiconducting SWNT was exposed to NO_2, its electrical resistance increased, while when a semiconducting SWNT was exposed to NH_3, the electrical resistance decreased [6]. These SWNT sensors exhibited fast response (2 s for 200 ppm NO_2 and 1 min for 1% NH_3), high sensitivity (the ratio of resistance after and before gas exposure was 1000 for NO_2 and 100 for NH_3) and low detection limits (2 ppm for NO_2 and 0.1% for NH_3) at room temperature. Reversibility was somewhat of an issue, as the sensors recovered slowly under ambient conditions or more quickly by heating to high temperatures. For molecules that do not modulate SWNT conductance directly, nanotube sidewalls can be modified with active components. For example, Dai et al. demonstrated that Pd nanoparticle-coated SWNTs could act as sensors for H_2 [7]. By decorating SWNTs with different components that are sensitive to specific gases, such as H_2S, F_2 or Cl_2, DNA-templated SWNTs could be developed as sensors for gases.

6.3 References

1. Huang, L.; Wind, S. J.; O'Brien, S. P. Controlled Growth of Single-Walled Carbon Nanotubes from an Ordered Mesoporous Silica Template, *Nano Lett*. **2003**, *3*, 299-303.
2. Zhang, Y.; Chang, A.; Cao, J.; Wang, Q.; Kim, W.; Li, Y.; Morris, N.; Yenilmez, E.; Kong, J.; Dai, H. Electric-Field-Directed Growth of Aligned Single-Walled Carbon Nanotubes, *Appl. Phys. Lett.* **2001**, *79*, 3155-3157.
3. Braun, E.; Eichen, Y.; Sivan, U.; Ben-Yoseph, G. DNA-Templated Assembly and Electrode Attachment of a Conducting Silver Wire, *Nature* **1998,** *391*, 775-778.
4. Becerril, H. A.; Stoltenberg, R. M.; Monson, C. F.; Woolley, A. T. Ionic Surface Masking for Low Background in Single- and Double-Stranded DNA-Templated Silver and Copper Nanorods, *J. Mater. Chem.* **2004,** *14*, 611-616.
5. Keren, K.; Berman, R. S.; Buchstab, E.; Sivan, U.; Braun, E. DNA-Templated Carbon Nanotube Field-Effect Transistor, *Science* **2003**, *302*, 1380-1382.
6. Kong, J.; Franklin, N.; Chou, C.; Pan, S.; Cho, K. J.; Dai, H. Nanotube Molecular Wires as Chemical Sensors, *Science*, **2000**, *287*, 622-625.
7. Kong, J.; Chapline, M.; Dai, H. Functionalized Single Walled Carbon Nanotubes for Molecular Hydrogen Sensors, *Adv. Mater.*, **2001**, *13*, 1384-1386.
8. Kong, J.; Yenilmez, E.; Tombler, T. W.; Kim, W.; Dai, H.; Laughlin, R. B.; Liu, L.; Jayanthi, C. S.; Wu, S. Y. Quantum Interference and Ballistic Transmission in Nanotube Electron Waveguides, *Phys. Rev. Lett.* **2001**, *87*, 106801-106804.